

The Massive Flat Space Limit of Cosmological Correlators

Sebastián Céspedes* and Sadra Jazayeri†

Department of Physics, Imperial College, London, SW7 2AZ, UK

Identifying useful *flat-space limits* for cosmological correlators, where they can be expressed in terms of observables in Minkowski space is nontrivial due to their scale-invariant nature. In recent years, it has been shown that *momentum-space* correlators encode flat-space amplitudes at specific singularities that emerge in the complex plane of their kinematics after analytical continuation. This flat-space limit is *massless* in the sense that the amplitude corresponds to the ultraviolet regime of the associated flat-space process, where the masses of the internal propagators are effectively zero. In this paper, we introduce a novel *massive flat-space (MFS) limit*, in which the internal masses in the corresponding flat-space Feynman graph remain finite. Our proposal applies to arbitrary graphs with light external legs and heavy internal lines, using a *double-scaling* limit. In this limit, the external energies, treated as independent variables, approach zero in inverse proportion to the propagator masses, which are sent to infinity. We present a general *reduction formula* that expresses diagrams in this limit in terms of amputated Feynman graphs in flat space. Our findings underscore the deep connections between the rich structure of *massive Feynman integrals* and the properties of cosmological correlators involving the exchange of heavy fields. Using this reduction formula, we compute sample one-loop contributions from heavy particles to inflationary correlators in the small sound-speed regime, revealing novel bispectrum shapes. The non-Gaussian signals we uncover, which are especially pronounced around the equilateral configuration, cannot be reproduced by adding local terms to the effective field theory of single-field inflation. Instead, they are captured by incorporating prescribed *spatially non-local* operators into the EFT.

*s.cespedes-castillo@imperial.ac.uk

†s.jazayeri@imperial.ac.uk

Contents

1	Introduction	2
1.1	Summary of the results	5
2	The Massive Flat-Space Limit	9
2.1	Recap: the Schwinger-Keldysh formalism	9
2.2	A reduction formula in the massive flat-space limit	14
2.3	From in-in integrals to the MFS limit	19
2.4	The MFS limit from the effective action in curved spacetime	25
2.5	Back to on-shell correlators with a reduced sound speed	30
3	Cosmological Phonon Collider	33
3.1	EFT of inflation and energy scales	33
3.2	Coupling matter fields to the EFT of inflation	35
3.3	Seed correlators from Mellin transformation	38
3.4	The bispectrum	42
4	Summary and Outlook	45
A	π Effective Action from Integrating Out The Heavy Field	47
B	Spectral Decomposition	47

1 Introduction

The fundamental observables in cosmology are the equal-time correlation functions of quantum fields at the end of inflation, commonly referred to as *Cosmological Correlators*. Their practical significance arises from the fact that we cannot directly observe the time evolution during inflation. Instead, what we can measure are the statistical properties of matter and radiation distributions at late times, which, following the classical evolution of the universe forward in time, can be derived from the universe’s wavefunction on the future boundary of the quasi-de Sitter spacetime during inflation. The correlators derived from the Born rule using this wavefunction encapsulate the integrated history of the universe during inflation within a single snapshot. At a more conceptual level, boundary correlators hold a special status because, in presence of dynamical gravity, observables are sharply defined only on the asymptotic boundaries of the relevant spacetime, such as the S-matrix in flat spacetime and CFT correlators in AdS. Cosmology is no exception to this principle, as good observables are likewise expected to be defined only on the asymptotic future boundary of the expanding universe [1]. In addition to these theoretical aspects, correlators are also of immense phenomenological importance, as they encode a wealth of information about the microscopic details of inflation, including its particle content, mass spectrum, interactions and potential clues about its UV completion (see, e.g., [2] and references therein).

In light of their phenomenological and theoretical significance, cosmological correlators have become a central topic of active research in recent years. Drawing inspiration from the remarkable successes of the scattering amplitude program, significant effort has been dedicated to identifying a set of optimal consistency conditions that enable the *bootstrapping* of these correlators. These conditions are typically derived from fundamental principles, including unitarity, locality, analyticity, and symmetries. [3–36]. This perspective, adopted in the *Cosmological Bootstrap* program [37], has led to an efficient formulation of correlators, circumventing some of the complexities encountered in the traditional in-in formalism, such as the challenging structure of nested time integrals. Using a diverse array of tools—including boundary differential equations [38–43], cutting rules [22, 44–47], Mellin transformations [48–51], recursion relations [20], dispersion relations [52–55], and spectral representations [56–60]—the bootstrap approach has significantly advanced our capacity to analytically decode the structure of cosmological correlators. This framework has also enabled the derivation of practical analytical expressions for correlators that are otherwise exceedingly difficult to obtain within the conventional bulk formalism (see, e.g., [61–79]).

A powerful consistency condition frequently used in the bootstrap program is the so-called *amplitude limit* of correlators. In perturbation theory, it has been demonstrated that as the *total energy* of a perturbative graph approaches zero, resulting in a singularity, the correlator becomes proportional to the on-shell scattering amplitude associated with the same diagram in flat space [10, 15, 19, 80, 81].

In more detail, consider a generic in-in diagram contributing to the n -point function of a massless field in momentum space, as depicted in Figure 1. The blob in the figure represents an

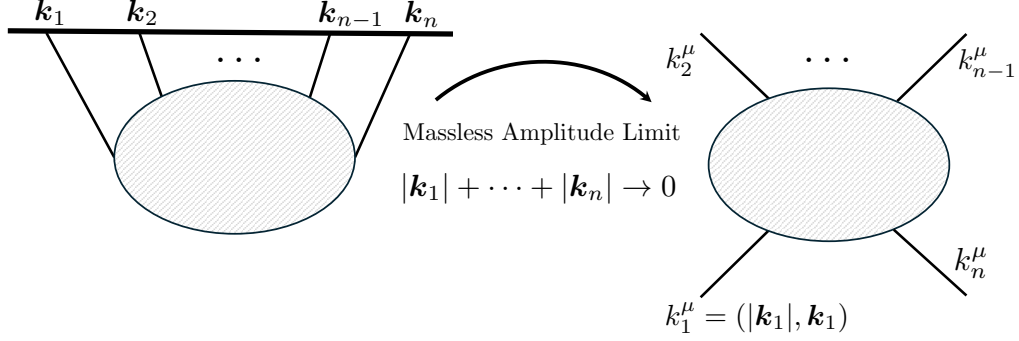


Figure 1: The amplitude limit of correlators, Eq. (1.3).

arbitrary structure of vertices and internal lines. This n -point function can be expressed as

$$\langle \phi(\mathbf{k}_1)\phi(\mathbf{k}_2)\dots\phi(\mathbf{k}_n) \rangle = F_n(\mathbf{k}_i)(2\pi)^3\delta^3\left(\sum_{i=1}^n \mathbf{k}_i\right), \quad (1.1)$$

where \mathbf{k}_i are the external momenta of the fields. Assuming the Bunch-Davies initial condition in the distant past, $F_n(\mathbf{k}_i)$ remains finite for all real-valued external kinematics, i.e., $\mathbf{k}_i \in \mathbb{R}^3$. However, upon analytic continuation as a function of $k_i = |\mathbf{k}_i|$ (also referred to as the external energies¹), $F_n(\mathbf{k}_i)$ exhibits a distinct type of singularity. This singularity arises when the total energy of the graph, defined as

$$k_T = \sum_{i=1}^n k_i, \quad (1.2)$$

approaches zero. Near this limit, F_n exhibits the following behavior [15]:

$$\lim_{k_T \rightarrow 0} F_n(\mathbf{k}_i) \propto \text{Re} \left\{ \frac{i^{n+1}}{(i k_T)^{\Delta_T}} \mathcal{A}(k_1^\mu, \dots, k_n^\mu) \right\}, \quad (1.3)$$

where k_i^μ are the following set of fictitious null four-momenta:

$$k_i^\mu = (k_i, \mathbf{k}_i), \quad (1.4)$$

which characterize the incoming particles in the flat-space scattering process associated with the same graph. $\mathcal{A}(k_i^\mu)$ represents the corresponding n -point scattering amplitude, and Δ_T quantifies the degree of divergence of the total energy singularity. Dimensional analysis implies that [19]

$$\Delta_T = 1 + \sum_{a=1}^V (\Delta_a - 4), \quad (1.5)$$

where Δ_a is the mass dimension of the operator acting at the a -th vertex².

¹Although energy is not conserved in an expanding background, the terminology remains useful when considering the flat-space limit, where time-translation symmetry is approximately restored, allowing a comoving energy to be assigned to each mode.

²For $\Delta_T = 0$, F_n exhibits a logarithmic divergence as $k_T \rightarrow 0$. In contrast, for $\Delta_T < 0$, while F_n remains finite near $k_T = 0$, its $(-\Delta_T)$ -th derivative with respect to k_T eventually becomes singular.

It is important to note that the amplitude appearing as the residue of the singularity in Eq. (1.3) is the UV limit of the corresponding scattering process in flat space. This implies that the propagators in the internal lines of the associated Feynman graph are massless, allowing the limit to also be termed the *massless flat-space limit* of correlators.

The aim of this work is to define an alternative flat-space limit of correlators in which the propagator masses remain nonzero (see [82], for a recent work in this direction). Preserving information about the masses in the flat-space limit offers several advantages. Conceptually, it enables us to explore how the rich structure of massive Feynman integrals (see, e.g., [83–86]) is encoded in cosmological correlators. As discussed previously, the standard flat-space high-energy limit causes all massive exchange processes to become degenerate with massless exchanges, which possess a much simpler analytical structure. Thus, identifying an alternative limit that avoids this degeneracy is highly desirable. Furthermore, from a bootstrap perspective, the analytical expressions for correlators involving massive exchanges are parameterized by both external momenta and the masses of internal propagators. Thus, a flat-space limit that is sensitive to variations in the mass parameters would serve as a significantly more powerful constraint on such correlators compared to the amplitude limit.

Finally, the *massive flat-space limit* developed in this work provides a practical tool for extracting observational signals imprinted by massive fields on the correlation functions of scalar fluctuations with reduced sound speed, $c_s \ll 1$. In particular, we focus on massive one-loop contributions to inflationary observables, such as the bispectrum. Phenomenologically, calculating one-loop contributions is crucial because they capture the leading-order effects of exchanging various species during inflation, such as fermions and charged bosons, which do not couple to curvature perturbations at tree level³. Such contributions might also be enhanced by additional color factors.

Recently, there has been significant interest in the *cosmological collider signal* left by such massive fields on inflationary correlators. This signal encodes the quantum oscillations of heavy fields on super-Hubble scales, manifesting as characteristic oscillatory features in specific soft limits of the bispectrum and trispectrum (see, e.g., [9, 97–121]). Despite significant progress in this field, exact results for massive loop diagrams, especially beyond the squeezed limit of the bispectrum or the collapsed limit of the trispectrum, remain limited due to the mathematical complexity of massive exchange processes. For recent advancements in massive bubble diagrams, see [58, 75].

In this work, using a reduction formula in our newly proposed flat-space limit, we compute novel one-loop contributions from massive scalars to inflationary correlators (Fig. 11), particularly the bispectrum. Our computation works in the regime where the scalar fluctuations propagate at a small speed of sound, i.e., $c_s \ll 1$, and the mass of the exchanged scalar lies within the window $H \ll m \lesssim \mathcal{O}(1)H/c_s$; see [62, 69, 122], for recent studies of this limit at tree-level.

Since we focus on the heavy limit of the exchanged field, our computation does not capture the squeezed-limit cosmological collider oscillations, as these are exponentially suppressed by the Boltzmann factor $\exp(-\pi m/H)$. However, we uncover intriguing features in the one-loop-induced

³In this work, we do not discuss one-loop effects induced by light fields and their infrared divergences. The interested reader may refer to, e.g., [87–96].

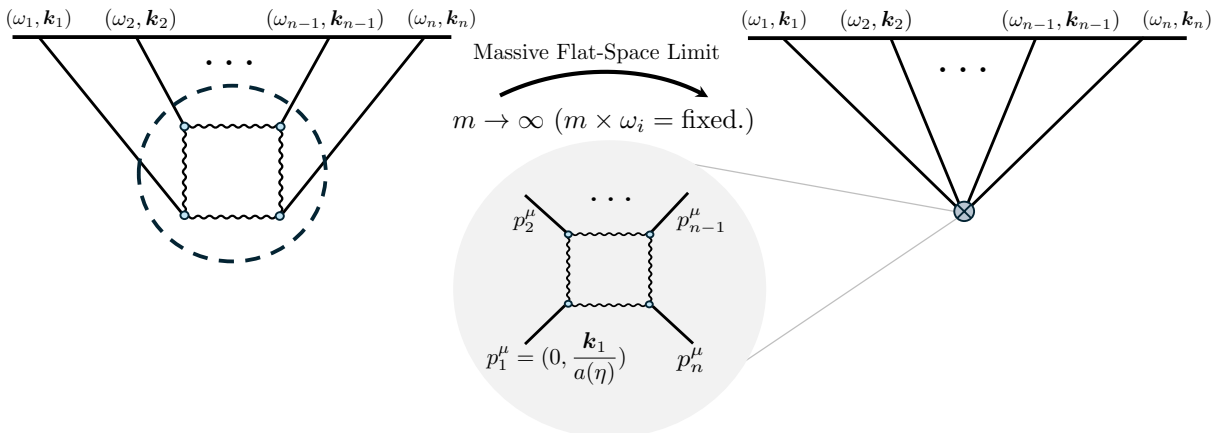


Figure 2: The massive flat-space limit of off-shell diagrams.

bispectrum around the equilateral configuration that cannot be replicated by simply adding local operators to the EFT action. Instead, we demonstrate that these features can be reproduced by introducing specific *non-local* operators into the EFT of single-field inflation.

The rest of the paper is organized as follows. In the next subsection, we summarise our *Massive Flat-Space (MFS) Limit* and the elements that goes into its proof for the reader's convenience. These will be discussed in full detail in Section 2. In this section, after reviewing the in-in formalism, we present a reduction formula that relates the correlator in the MFS limit to specific massive Feynman diagrams in flat space. In Section 2.3, we prove our reduction formula by directly taking the MFS limit of the in-in expressions for two specific examples, namely the tree-level exchange and the one-loop, bubble graph (in Appendix B, for the one-loop example, we provide another proof of the MFS behaviour based on the Källén–Lehmann representation of composite operators). In Section 2.4, exploiting the Wilsonian effective action formalism in dS, we provide a general proof for the reduction formula for an arbitrary graph with heavy internal lines. Section 2.5 proposes an analogous reduction formula for correlators of scalar fluctuations in the EFT of inflation (relations to a non-local EFT of single-field inflation is discussed in Appendix A). This reduction formula will be exploited in Section 3 to compute the bispectrum induced by the tree-level and one-loop exchanges of heavy fields, in the $c_s \rightarrow 0$ limit.

1.1 Summary of the results

Before discussing our massive flat-space limit, let us briefly review why masses vanish in the amplitude limit by studying a tree-level example (see Fig. 3). Consider the four-point function of a conformally coupled field ϕ induced by the single exchange of a heavy scalar σ , assuming that they interact via the cubic operator $\phi^2 \sigma$. The s -channel component of this diagram is given by

$$F_4(k_1, k_2, k_3, k_4, s) = \sum_{\pm\pm} (\pm i)(\pm i) \int_{-\infty(1\mp i\epsilon)}^0 \frac{d\eta}{\eta^2} \frac{d\eta'}{\eta'^2} e^{\pm i(k_1+k_2)\eta} e^{\pm i(k_3+k_4)\eta'} G_{\pm\pm}(s, \eta, \eta'), \quad (1.6)$$

where η, η' are the conformal times attached to the vertices, and $G_{\pm\pm}(s, \eta, \eta')$ are the *bulk-to-bulk* propagators associated with the heavy field, given by Eq. (2.4), with $s = |\mathbf{k}_1 + \mathbf{k}_2|$ denoting the exchanged momentum.

It is useful to expand the integrand around the conformal time corresponding to one of the vertices, e.g., η , by substituting $\eta' = \eta + \Delta\eta$. As we approach $k_T = 0$, the $++$ and $--$ contributions to F_4 are the only components that become singular. The singular behavior of these components is dictated by the early-time limit of the integrand, that is, when $\eta \propto k_T^{-1} \rightarrow -\infty$, while $\Delta\eta$ is maintained finite. In this early-time limit,

$$\lim_{k_T \rightarrow 0} F_4 \propto \text{Re} \left[\int_{-\infty(1-i\epsilon)}^0 \frac{d\eta}{\eta^4} e^{ik_T\eta} \left(\int_{-\infty}^{+\infty} d\Delta\eta e^{i(k_3+k_4)\Delta\eta} G_{++}(s, \eta, \eta + \Delta\eta) \right) \right]. \quad (1.7)$$

Within the bulk-to-bulk propagators G_{++} above, the conformal time η is taken to $-\infty$. Therefore, in this limit, the mass of the propagator becomes negligible compared to its blue-shifted physical kinetic energy, defined by $E = H|s\eta|$, where H is the Hubble rate. This implies that the Hankel functions appearing in the propagators (Eq. (2.6)) can be well approximated by massless plane-waves in flat space. Consequently, as long as we are concerned with the leading order singular behaviour around $k_T = 0$, we can effectively replace the time-ordered propagator with

$$G_{++}(s, \eta, \eta + \Delta\eta) \rightarrow H^2 \eta^2 G_F(s, 0, \Delta\eta), \quad (1.8)$$

where G_F is the *massless Feynman propagator* in flat space,

$$G_F(s, \eta_1, \eta_2) = \frac{1}{2s} \left(e^{-is(\eta_1 - \eta_2)} \theta(\eta_1 - \eta_2) + \eta_1 \leftrightarrow \eta_2 \right). \quad (1.9)$$

Substituting the asymptotic form of the propagator inside the parenthesis (...) in Eq. (1.7), along with the incoming plane wave $\exp(i(k_3 + k_4)\Delta\eta)$, reproduces the on-shell two-to-two amplitude with vanishing internal and external masses, namely

$$\mathcal{A}_4 = \frac{1}{-(k_1 + k_2)^2 + (\mathbf{k}_1 + \mathbf{k}_2)^2 + i\epsilon} = \frac{1}{(k_1^\mu + k_2^\mu)^2 + i\epsilon}. \quad (1.10)$$

Meanwhile, the rest of the integrand, i.e., $\int \frac{d\eta}{\eta^4} \times \eta^2 e^{ik_T\eta}$, generates the expected singular behaviour, corresponding to $\Delta_T = -1$.

Heavy off-shell graphs. Our proposal for a massive flat-space limit applies to *heavy graphs*, which are defined by in-in diagrams with light external legs and heavy internal lines (see Fig. 2). For simplicity, we assume that all internal lines share the same mass, $m \geq 3H/2$, while the external legs are light, often corresponding to massless or conformally coupled fields. Such *on-shell* correlators are characterized by the momenta associated with its external fields, i.e., \mathbf{k}_i . To define our flat-space limit, we first define an *off-shell* extension of such graphs by adding a set of fictitious energy variables ω_i to the list of the external kinematics (see also [54]). This is naturally achieved by replacing the Schwinger-Keldysh bulk-to-boundary propagators $K^\pm(k_i, \eta)$ with $K^\pm(\omega_i, \eta)$, where ω_i is an independent variable, i.e., $\omega_i^2 \neq \mathbf{k}_i^2$. To each on-shell correlator $F_n(\{\mathbf{k}_i\})$, this replacement assigns a unique function of ω_i , denoted by

$$F_n(\omega_i, \mathbf{k}_i; m) \quad (i = 1, \dots, n). \quad (1.11)$$

These functions define correlators that are off-shell in the sense that their external propagators do not satisfy the equations of motion, i.e., $\square(K(\omega_i, \eta) \exp(i\mathbf{k}_i \cdot \mathbf{x})) \neq 0$, in contrast with one-shell

diagrams with external legs that satisfy $\square(K(k_i, \eta) \exp(i\mathbf{k}_i \cdot \mathbf{x})) = 0$.

The Massive Flat-Space Limit. We consider the following *double-scaling limit* of a heavy graph:

$$m/H \rightarrow \infty, \quad \frac{\omega_i}{|\mathbf{k}_i|} \rightarrow 0, \quad \text{while} \quad \frac{\omega_i}{|\mathbf{k}_i|} \times \frac{m}{H} = \text{finite}. \quad (1.12)$$

In this limit, we show that F_n asymptotes to

$$F_n \left(\omega_i, \mathbf{k}_i; \frac{m}{H} \right) \xrightarrow{\text{MFS}} F_n^{\text{MFS}}(\omega_i, \mathbf{k}_i; m) (1 + \mathcal{O}(H/m)), \quad (1.13)$$

where F_n^{MFS} is a contact diagram in de Sitter, given by

$$F_n^{\text{MFS}}(\omega_i, \mathbf{k}_i; m) = 2 \text{Re} \int_{-\infty(1-i\epsilon)}^0 \frac{d\eta}{H^4 \eta^4} G_n[p_1^\mu(\eta), \dots, p_n^\mu(\eta); m] \prod_{i=1}^n O_n(\partial_\eta, \eta, \mathbf{k}_i) K^+(\omega_i, \eta). \quad (1.14)$$

In this *reduction formula*, $O_n(\dots)$ are derivative operators acting on the external legs, which are inherited from the original in-in diagram. p_i^μ represent a set of (time-dependent) off-shell four-momenta, given by

$$p_i^\mu(\eta) = (0, -H \mathbf{k}_i \eta) \quad (i = 1, \dots, n), \quad (1.15)$$

which characterize n external legs of a dual Feynman graph in flat space (see Fig. 2). This Feynman graph is obtained by amputating the external lines of the original in-in diagram, and is given by $G_n(p_i^\mu; m)$. The rules for computing G_n are the familiar Feynman rules in flat space: four-momentum is conserved at each vertex; each undetermined momentum brings a factor of $\int d^4 q_l$ (where q_l is the loop four-momentum), and each internal line is assigned a massive Feynman propagator $\frac{-i}{q^2 + m^2}$.

For the tree-level exchange example above (Eq. (1.6)), the MFS reduction formula gives

$$\lim_{\text{MFS}} F_4(\omega_i, k_i, s) = 2 \text{Im} \int_{-\infty(1-i\epsilon)}^0 d\eta \frac{1}{H^2 s^2 \eta^2 + m^2} \exp(i\omega_T \eta). \quad (1.16)$$

As another example, consider the one-loop, four-point function induced by the $\phi^2 \sigma^2$ interaction (see Fig. 3 and Eq. (2.13)). The MFS limit of this loop diagram is given by

$$\begin{aligned} \lim_{\text{MFS}} F_4(\omega_i, k_i, s) &= \frac{-1}{16\pi^2} \text{Re} \int_{-\infty}^0 d\eta \left(\int_0^1 dx \log \left[\frac{m^2 + x(1-x)H^2 s^2 \eta^2}{\mu^2} \right] \right) \exp(i\omega_T \eta) \\ &+ \frac{1}{8\pi^2} \left(-\frac{1}{(d-4)} + \frac{1}{2} \log(4\pi e^{-\gamma_E}) \right) \frac{1}{\omega_T}, \end{aligned} \quad (1.17)$$

where the UV divergence of the associated loop graph G_4 is regulated in dim reg, and μ is the corresponding renormalization scale. In the $d \rightarrow 4$ limit, the second line above is a divergent local contribution that is canceled by adding a $g_4 \phi^4$ counter-term to the action, using the $\overline{\text{MS}}$ scheme

In summary, the reduction formula indicates that in the MFS limit, any heavy graph, regardless of its internal structure, simplifies to a contact diagram. The time-dependent vertex of this diagram is determined by the corresponding amputated flat-space graph with red-shifted external momenta.

Elements of the proof. Let us sketch the proof of the reduction formula, which is based on two observations. First of all, in the heavy limit, the mode functions of the massive field can be replaced by its WKB approximation, namely

$$\sigma_+^{\text{WKB}}(s, \eta) \propto \frac{1}{a(\eta)} \left(s^2 + \frac{m^2}{H^2 \eta^2} \right)^{-1/4} \exp \left(-i \int_{-\infty}^{\eta} d\eta' \sqrt{s^2 + \frac{m^2}{H^2 \eta'^2}} \right), \quad (1.18)$$

For large masses, this formula can be used to simplify the in-in integrals because the WKB approximation is valid during the entire evolution, from $\eta = -\infty$ all the way to $\eta = 0$. The fast oscillations of the WKB mode function as $m \rightarrow \infty$ implies that the multi-dimensional in-in integral peaks at a region where the vertices (η_a) are clustered around a central conformal time η , i.e.,

$$\left| \frac{1}{H \eta} (\eta_a - \eta) \right| \lesssim \mathcal{O}(1) \frac{1}{m}. \quad (1.19)$$

This is the fundamental reason why taking the MFS limit collapses the internal structure of the diagram into a single vertex.

The second observation is that, in the MFS limit, taking $\omega_T = \sum \omega_i \rightarrow 0$ serves a similar purpose as taking $k_T \rightarrow 0$ in the amplitude limit: it effectively pushes all the vertices η_a to $-\omega_T^{-1} \rightarrow -\infty$. However, a key difference arises: in this limit, the mass of the propagators cannot be ignored. This is because, in the early time limit, the physical kinetic energy of each internal line scales inversely with $1/\omega_T$, making it proportional to the mass. Specifically,

$$E = -Hs\eta \rightarrow \frac{Hs}{\omega_T} \propto m, \quad (1.20)$$

where s is the norm of the internal line comoving momentum. In Section 2 and Appendix B we use these two ingredients to prove the reduction formula in three different ways, namely (i) by directly taking the MFS limit of the in-in integrals, (ii) using the Wilsonian effective action formalism and finally, for the bubble diagram, (iii) using a spectral decomposition approach.

Conventions. We chart the de Sitter Poincaré patch using the following coordinates

$$ds = a^2(\eta)(-d\eta^2 + d\mathbf{x}^2), \quad a(\eta) = -\frac{1}{\eta H}, \quad (1.21)$$

where H is the Hubble constant, and $\eta \in (-\infty, 0)$ is the conformal time. We sometimes also use the FLRW format of the metric, expressed as

$$ds^2 = -dt^2 + a^2(t)d\mathbf{x}^2, \quad (1.22)$$

where in de Sitter we have $a = \exp(Ht)$. Prime on fields, e.g. π' , denotes derivative with respect to η , while dot will stand for derivative with respect to t . We use the following convention for the Riemann and Ricci tensors: $R^\mu_{\nu\alpha\beta} = \partial_\alpha \Gamma^\mu_{\beta\nu} + \dots$, and $R_{\mu\nu} = R^\alpha_{\mu\alpha\nu}$. We use bold letters to refer to spatial vectors, e.g., \mathbf{x} for spatial coordinates and \mathbf{k} for spatial momentum. We also use the notation

$$k_{ij} = k_i + k_j, \quad (1.23)$$

where $k_i = |\mathbf{k}_i|$. A massive scalar with mass m in dS_d is characterized by the following conformal weights

$$\Delta_\pm = \frac{d-1}{2} \pm i\mu, \quad \mu^2 = \frac{m^2}{H^2} - \frac{(d-1)^2}{4}. \quad (1.24)$$

The principal series (heavy fields) corresponds to $\mu > 0$, and complementary series (light fields) corresponds to $\mu = i\nu$ with $\nu > 0$. We collectively refer to the former fields with σ and the latter with ϕ , which includes both the conformally coupled field ($\Delta_+ = \frac{d-2}{2}$) and the massless field ($\Delta_+ = 0$). We also use the same symbol μ to refer to the renormalization scale, but the context will make the difference clear. A prime on a correlator indicate that the overall momentum-conserving delta function has been stripped off, i.e.,

$$\langle \phi(\mathbf{k}_1) \dots \phi(\mathbf{k}_n) \rangle = (2\pi)^3 \delta^{(3)} \left(\sum_{i=1}^n \mathbf{k}_i \right) \langle \phi(\mathbf{k}_1) \dots \phi(\mathbf{k}_n) \rangle'. \quad (1.25)$$

2 The Massive Flat-Space Limit

2.1 Recap: the Schwinger-Keldysh formalism

Let us begin by discussing how to obtain correlation functions from the path integral (see also [123]). The most practical approach involves defining a partition function by introducing external sources (or currents) to the path integral and taking functional derivatives with respect to these sources. In cosmology, where observations are made at finite times, the most suitable framework for this purpose is the *in-in* or Schwinger-Keldysh formalism.

In this formalism, the theory is assumed to start in the standard Bunch-Davies (BD) vacuum⁴, with observations made at a specific finite time η_0 , usually taken to be the end of inflation. Fields evolve forward in time from the initial vacuum state to η_0 along the upper branch of the Schwinger-Keldysh contour and then reverse-evolve back to the vacuum along the lower branch. The partition function is constructed by placing currents on each branch to act as sources for the fields. The evolution is governed by two path integrals: one over the bulk fields, describing their forward and backward evolution, and another over the field profiles at η_0 .

For a single scalar field with the action $S[\phi]$, the field evolves forward on the upper branch from the BD vacuum at $\eta \rightarrow -\infty$ all the way to the end of inflation, when it takes the profile $\phi(\eta_0) = \phi_0$. On the lower branch, the field evolves backward from the same profile ϕ_0 , returning

⁴Other vacua are possible, but we focus exclusively on the Bunch-Davies choice.

to the BD vacuum. To distinguish between the solutions on the two branches, we label them with + (upper branch) and - (lower branch) superscripts. The partition function is given by:

$$Z[J_+, J_-] = \int D\phi_0 \int_{\text{BD}}^{\phi_0} D\phi_+ \int_{\text{BD}}^{\phi_0} D\phi_- e^{iS[\phi_+] - iS[\phi_-] + i \int d^4x (\phi_+ J_+ - \phi_- J_-)}, \quad (2.1)$$

where, J_+ and J_- are external sources coupled to the fields on the respective branches. We assume that the bulk path integral is dominated by the classical solution $\phi_{\text{cl}}(\eta)$, which must satisfy the appropriate boundary conditions imposed by the path integral.

In order to build the propagators we will need the mode functions obtained from the action $S_0[\phi]$. For example, the positive-frequency mode functions for massless and conformally coupled scalar fields on the upper branch are:

$$\phi_+(k, \eta) = \frac{iH}{\sqrt{2k^3}}(1 + ik\eta)e^{-ik\eta} \quad (\text{massless}), \quad \phi_+(k, \eta) = -\frac{H}{\sqrt{2k}}\eta e^{-ik\eta} \quad (\text{conformally coupled}). \quad (2.2)$$

On the lower branch, the solutions are the complex conjugates of the upper branch mode functions.

The propagators can be derived from the free partition function by solving for the classical solutions sourced by the external currents on each branch. After substituting these solutions into the path integral and integrating over the field profile, we obtain:

$$Z_0 = \exp \left[-\frac{1}{2} \int_{\mathbf{k}} \int d\eta a^4(\eta) \int d\eta' a^4(\eta') (J_+(\eta)G_{++}(k, \eta, \eta')J_+(\eta') - J_+(\eta)G_{+-}(k, \eta, \eta')J_-(\eta') \right. \\ \left. - J_-(\eta)G_{-+}(k, \eta, \eta')J_+(\eta') + J_-(\eta)G_{--}(k, \eta, \eta')J_-(\eta') \right] \quad (2.3)$$

where the propagators expressed in terms of the mode functions are,

$$\begin{aligned} G_{++}(k, \eta, \eta') &= \phi_-(k, \eta')\phi_+(k, \eta)\theta(\eta - \eta') + \phi_-(k, \eta)\phi_+(k, \eta')\theta(\eta' - \eta), \\ G_{+-}(k, \eta, \eta') &= \phi_+(k, \eta')\phi_-(k, \eta), \\ G_{--}(k, \eta, \eta') &= \phi_+(k, \eta')\phi_-(k, \eta)\theta(\eta - \eta') + \phi_+(k, \eta)\phi_-(k, \eta')\theta(\eta' - \eta), \\ G_{-+}(k, \eta, \eta') &= \phi_-(k, \eta')\phi_+(k, \eta). \end{aligned} \quad (2.4)$$

Here, G_{++} and G_{--} are the time-ordered and the anti-time-ordered propagators on their respective branches, while G_{+-} and G_{-+} are Wightman propagators that mix the two branches. To include interactions, we split the action into a free part S_0 and an interacting part S_{int} . The full partition function can then be written as:

$$Z[J_+, J_-] = e^{iS_{\text{int}}\left[\frac{\delta}{\delta J_+}\right] - iS_{\text{int}}\left[\frac{\delta}{\delta J_-}\right]} Z_0[J_+, J_-], \quad (2.5)$$

where the free partition function is given in (2.3).

This formalism can be easily extended to include fields with different masses and spins. In addition to a massless or a conformally coupled field, we will also consider a massive scalar field

σ with mass m . In four dimensions the corresponding mode functions are given by:

$$\begin{aligned}\sigma_+(k\eta) &= \frac{\sqrt{\pi}H}{2} e^{-\pi\mu/2+i\pi/4} (-\eta)^{3/2} H_{i\mu}^{(1)}(-k\eta), \\ \sigma_-(k\eta) &= \frac{\sqrt{\pi}H}{2} e^{\pi\mu/2-i\pi/4} (-\eta)^{3/2} H_{i\mu}^{(2)}(-k\eta),\end{aligned}\tag{2.6}$$

where $\mu = \sqrt{\frac{m^2}{H^2} - \frac{9}{4}}$. Fields in the principal series representation have $m^2 \geq \frac{9H^2}{4}$, such that μ is real, whereas for the complementary series $m^2 \leq \frac{9H^2}{4}$, μ is imaginary.

In general, a systematic set of Feynman rules can be set up for computing cosmological correlators. External lines are represented by the bulk-to-boundary propagators as given in K^+ and K^- ,

$$K^+(k, \eta) = \phi_+(k, \eta_0)\phi_-(k, \eta), \quad K^-(k, \eta) = \phi_-(k, \eta_0)\phi_+(k, \eta),\tag{2.7}$$

while internal lines correspond to the bulk-to-bulk propagators as defined in (2.4). For each vertex, a volume factor of $a^4(\eta)$ is included, along with a time integral that runs from $\eta \rightarrow -\infty$ up to the observation time η_0 . These rules can be readily generalized to interactions involving derivatives by applying the appropriate differential operators directly to the corresponding propagators.

We focus on in-in diagrams with external lines representing light fields (e.g., massless or conformally coupled fields) and internal lines corresponding to heavy fields (with $\mu > 0$). Such diagrams will be referred to as *heavy graphs*. To calculate these diagrams, we consider a partition function that depends on four external sources, namely $J_{\pm}^{\phi}, J_{\pm}^{\sigma}$. A generic n -point correlator of the light field, which we denote by ϕ , can then be expressed as follows:

$$\langle \phi(\mathbf{k}_1) \dots \phi(\mathbf{k}_n) \rangle = (-i)^n \frac{\delta^n}{\delta J_+^{\phi}(\mathbf{k}_1) \dots \delta J_+^{\phi}(\mathbf{k}_n)} Z[J_+^{\phi}, J_+^{\sigma}, J_-^{\phi}, J_-^{\sigma}] \Big|_{J_{\pm}^{\phi, \sigma} = 0}\tag{2.8}$$

The derivatives with respect to the external sources will bring down bulk-to-boundary propagators of ϕ whereas the interaction appearing in the partition function will bring down bulk-to-boundary propagators of σ . The contribution from a heavy diagram with \mathcal{V} vertices and \mathcal{I} internal lines then becomes

$$\begin{aligned}\langle \phi(\mathbf{k}_1) \dots \phi(\mathbf{k}_n) \rangle' \supset & \sum_{\pm_1, \pm_2, \dots, \pm_{\mathcal{V}}} \left(\prod_{a=1}^{\mathcal{V}} (\pm_a i \lambda_a) \int d\eta_a a^4(\eta_a) \right) \prod_{i=1}^n O_i(\mathbf{k}_i, \frac{\partial}{\partial \eta_{d_i}}, \eta_{d_i}) K_{\phi}^{\pm d_i}(k_i, \eta_{d_i}) \\ & \times \left(\prod_{l=1}^{\mathcal{L}} \int \frac{d^3 \mathbf{q}_l}{(2\pi)^3} \right) \prod_{\text{internal lines}(b,c)} O_{bc}(\mathbf{q}_{bc}, \eta_b, \eta_c, \partial_{\eta_b}, \partial_{\eta_c}) G_{\pm_b, \pm_c}^{\sigma}(\mathbf{q}_{bc}, \eta_b, \eta_c),\end{aligned}\tag{2.9}$$

where we have indexed the vertices by $a = 1, \dots, \mathcal{V}$, λ_a are the associated coupling constants, and $1 \leq d_i \leq \mathcal{V}$ ($i = 1, \dots, n$) are a set of integers that specifies the vertex to which the i -th

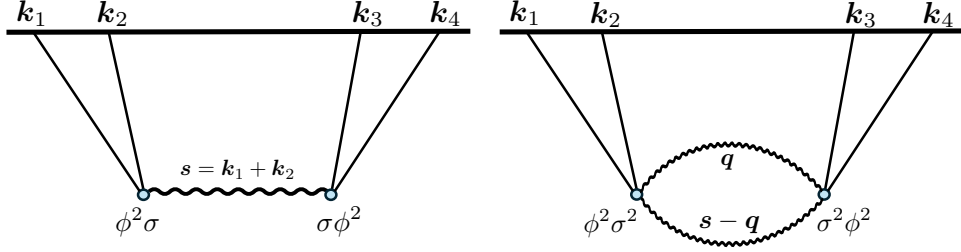


Figure 3: The scalar-exchange (SE) and scalar one-loop, bubble diagram (SB) diagrams contributing to the four-point function of the conformally coupled field.

external leg is connected. Vertices can be of $+$ or $-$ types, depending on which an appropriate bulk-to-bulk or bulk-to-boundary propagators is included. \mathbf{q}_l ($l = 1, \dots, \mathcal{L}$) represent the loop momenta, with $\mathcal{L} = \mathcal{I} - \mathcal{V} + 1$ denoting the number of loops. The three-momenta associated with the internal line connecting vertex b to vertex c are denoted by \mathbf{q}_{bc} , which are determined by momentum conservation in terms of the external and loop momenta. The operators O_n describe derivatives at the vertices acting on the external legs, while O_{ab} captures any derivatives acting on the internal lines.

Notice that the ordering of the time integrals is not arbitrary but is dictated by the causal structure of the bulk-to-bulk propagators. For simplicity, we drop the σ label from the bulk-to-bulk propagators, as internal lines always involve σ .

Four-point functions of the conformally coupled field. Using the Feynman rules introduced above, we derive the in-in expression for two specific diagrams of interest: the single-exchange diagram and the one-loop bubble diagram, both contributing to the four-point function of a conformally coupled (cc) field (see Figure 3). To construct these diagrams, consider the following cubic and quartic interactions between a cc field ϕ and a heavy scalar σ :

$$\mathcal{L}_{\text{int}} = a^4(\eta) (-g \phi^2 \sigma - g' \phi^2 \sigma^2) . \quad (2.10)$$

Using these vertices we can form a single-exchange and a one-loop, bubble graph. The corresponding four-point functions in the s -channel can be expressed as

$$\begin{aligned} \langle \phi(\mathbf{k}_1) \phi(\mathbf{k}_2) \phi(\mathbf{k}_3) \phi(\mathbf{k}_4) \rangle'_{\text{SE}} &= \frac{\eta_0^4}{4k_1 k_2 k_3 k_4} g^2 F_{\text{SE}}(k_{12}, k_{34}, s) + t, u\text{-channels} && \text{(Scalar-Exchange)}, \\ \langle \phi(\mathbf{k}_1) \phi(\mathbf{k}_2) \phi(\mathbf{k}_3) \phi(\mathbf{k}_4) \rangle'_{\text{SB}} &= \frac{\eta_0^4}{2k_1 k_2 k_3 k_4} g'^2 F_{\text{SB}}(k_{12}, k_{34}, s) + t, u\text{-channels} && \text{(Scalar-Bubble)}. \end{aligned} \quad (2.11)$$

where $F_{\text{SE}, \text{SB}}$, which are functions of the three variables $k_{12} = k_1 + k_2$, $k_{34} = k_3 + k_4$ and $s = |\mathbf{k}_1 + \mathbf{k}_2|$, are given by

$$F_{\text{SE,SB}}(k_{12}, k_{34}, s) \equiv F_{\text{SE,SB}}^{++} + F_{\text{SE,SB}}^{+-} + F_{\text{SE,SB}}^{-+} + F_{\text{SE,SB}}^{--},$$

with

$$F_{\text{SE}}^{\pm\pm} = (\pm i)(\pm i) \int_{-\infty(1\mp i\epsilon)}^0 \frac{d\eta}{\eta^2} \frac{d\eta'}{\eta'^2} e^{\pm ik_{12}\eta} e^{\pm ik_{34}\eta'} G_{\pm\pm}(s, \eta, \eta'), \quad (2.12)$$

$$F_{\text{SB}}^{\pm\pm} = (\pm i)(\pm i) \int_{-\infty(1\mp i\epsilon)}^0 \frac{d\eta}{\eta^2} \frac{d\eta'}{\eta'^2} e^{\pm ik_{12}\eta} e^{\pm ik_{34}\eta'} \int \frac{d^3\mathbf{q}}{(2\pi)^3} G_{\pm\pm}(|\mathbf{q}|, \eta, \eta') G_{\pm\pm}(|-\mathbf{q} + \mathbf{s}|, \eta, \eta'). \quad (2.13)$$

In Section 3.4, we will use the above four-points to compute the bispectrum of curvature perturbations by applying appropriate weight-shifting operators, transforming the external conformally coupled fields into massless ones.

The Effective Action

When considering heavy graphs introduced above, a natural expectation is that as the internal masses become very large, the complicated structure of in-in time integrals should simplify. Drawing from the more familiar in-out computations, integrating out a massive field σ is expected to yield an effective action. At low energies, this effective action typically contains a series of local operators with an increasing number of derivatives, suppressed by the mass scale of the integrated-out field.

Extending the same EFT concept to the in-in formalism introduces subtleties, particularly in how boundary conditions are applied to the path integral [54, 124–127]. A key distinction when integrating out massive fields in the in-in versus in-out formalisms lies in the structure of the propagators. While the effective action in the in-out formalism involves only time-ordered propagators, the in-in framework also includes non-time-ordered propagators. These additional components account for non-unitary effects arising from interactions between the two branches of the in-in contours and must be incorporated into the effective action.

To illustrate this, we consider the interaction $g'\phi^2\sigma^2$. To construct the correct effective action for ϕ , one must solve the path integral for σ while accounting for both branches of the in-in contour. The effective action is then formally expressed as:

$$e^{iS_{\text{eff}}[\phi_+, \phi_-]} = \int D\sigma \int_{BD}^{\sigma} D\sigma_1 \int_{BD}^{\sigma} D\sigma_2 e^{iS[\phi_+, \sigma_+] - S[\phi_-, \sigma_-]}. \quad (2.14)$$

Notice that the path integrals over σ_+ and σ_- are identified at their endpoints, leading to an effective action that generally mixes terms containing ϕ_+ and ϕ_- . This type of action, often referred to as “non-unitary,” cannot be derived from a conventional Hamiltonian. For the example considered here, the resulting effective action contains terms like:

$$S_{\text{eff}}[\phi_+, \phi_-] \supset \int a^4(\eta) d^3\mathbf{x} \int a^4(\eta') d^3\mathbf{y} \sum_{\pm, \pm} \phi_{\pm}(\mathbf{x}, \eta)^2 G_{\pm, \pm}(|\mathbf{x} - \mathbf{y}|, \eta, \eta')^2 \phi_{\pm}(\mathbf{y}, \eta')^2, \quad (2.15)$$

which captures the complete propagator structure, maintaining consistency with the in-in formalism and accurately reproducing the correlators in Eq. (2.13).

The effective action (2.15) in its current form is non-unitary and fully non-local, making it not very useful for simplifying the correlator, i.e., in this case the scalar bubble graph. We will demonstrate that certain simplifications arise in the massive flat space limit. First, by taking the mass of the exchanged field to infinity, we argue that the contributions from the non-time-ordered propagators $G_{\pm\mp}$ become exponentially small due to the rapid oscillations of the massive propagators in the WKB approximation, so we can use the unitary part of this effective action. Furthermore, in the MFS limit, we show that the corresponding bubble graph receives its dominant contribution from near the diagonal $\eta = \eta'$ of the in-in time integral, allowing the effective action to also be expanded around $\eta = \eta'$, making it local in time, although still non-local in space. We clarify these points in Section 2.4.

2.2 A reduction formula in the massive flat-space limit

In this section, we introduce a new flat space limit for diagrams involving heavy internal lines. We then derive a universal reduction formula that governs the behavior of correlators in this limit. Additionally, we analyze a tree-level example and highlight the distinction between our limit and the conventional amplitude limit.

Off-shell correlators and the MFS limit

To establish our limit, it is convenient to work with a set of *off-shell* correlators. These are defined within perturbation theory using the same diagrammatic rules outlined in the previous section, with one crucial modification: a fictitious energy variable ω_i is introduced into the bulk-to-boundary propagators, treated as independent of \mathbf{k}_i , i.e., $\omega_i^2 \neq \mathbf{k}_i^2$. For related constructions of off-shell wavefunction coefficients, see [54]⁵. In practice, this amounts to the following substitution inside the in-in integrand

$$K^+(k_i, \eta) \rightarrow K^+(\omega_i, \eta), \quad (2.16)$$

while keeping the bulk-to-bulk propagators unchanged. Following this substitution, to each n -point diagram one can assign a unique function of the external energies ω_i , given by

$$F_n(\mathbf{k}_i) \rightarrow F_n(\omega_i, \mathbf{k}_i), \quad (2.17)$$

which we will refer to by the off-shell correlator associated with that graph. The terminology is appropriate because the plane-wave defined by $K^+(\omega, \eta) \exp(i\mathbf{k}\cdot\mathbf{x})$ does not satisfy the equation of motion for the free theory, unless it is brought on-shell by setting $\omega_i = k_i$.

We now focus on *heavy graphs*, defined as graphs with light external legs and vertices connected solely by heavy internal lines, where the masses of the internal lines lie within the de Sitter principal series. For simplicity, we consider scalar fields and assume that all internal lines have the same mass m . However, we expect that our results extend to graphs with internal lines of varying spins and masses.

⁵We thank Scott Melville for insightful discussions on the off-shell extension of cosmological correlators.

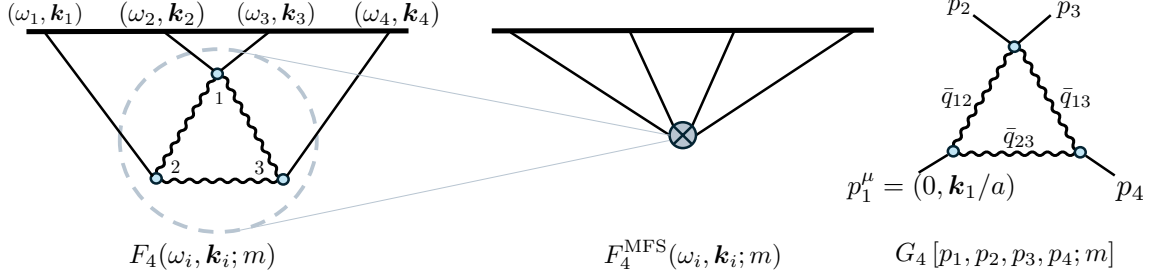


Figure 4: An illustration of the elements involved in the MFS limit reduction formula (2.20) for a one-loop graph of the four-point function with three vertices (*left*). $p_i^\mu = (0, \mathbf{k}_i/a)$ ($i = 1, \dots, 4$) represent a set of fictitious four-momenta that characterize the amputated graph in flat-space (*right*). \bar{q}_{bc} ($b, c = 1, 2, 3$) denote the internal line four-momenta of this graph, which can be expressed in terms of the loop momentum \bar{q} and the p_i 's, i.e., $\bar{q}_{12} = q$, $\bar{q}_{13} = p_2 + p_3 - q$, and $\bar{q}_{23} = q + p_1$. In the MFS limit, the correlator reduces to a contact diagram (*middle*), with its vertex corresponding to the amputated Feynman diagram.

For these heavy graphs, we introduce the *Massive Flat-Space (MFS)* limit, defined as:

$$\frac{\omega_i}{|\mathbf{k}_i|} \rightarrow 0^+, \quad \frac{m}{H} \rightarrow +\infty, \quad \text{while} \quad \frac{m}{H} \times \frac{\omega_i}{|\mathbf{k}_i|} = \lambda_i < \infty. \quad (2.18)$$

In the MFS limit, we propose that an off-shell heavy graph F_n reduces to a contact diagram with a vertex that is determined by a Feynman diagram in flat space, which is obtained by amputating the external legs (see Fig. 4).

In more detail, in the MFS limit F_n asymptotes to

$$F_n \left(\omega_i, \mathbf{k}_i; \frac{m}{H} \right) \xrightarrow{\text{MFS}} F_n^{\text{MFS}}(\omega_i, \mathbf{k}_i; m) (1 + \mathcal{O}(H/m)), \quad (2.19)$$

where F_n^{MFS} is given by the following *reduction formula*:

$$F_n^{\text{MFS}}(\omega_i, \mathbf{k}_i; m) = 2 \text{Re} \int_{-\infty(1-i\epsilon)}^0 d\eta a^4(\eta) G_n[p_1^\mu(\eta), \dots, p_n^\mu(\eta); m] \prod_{i=1}^n O_n(\partial_\eta, \eta, \mathbf{k}_i) K^+(\omega_i, \eta). \quad (2.20)$$

Here, the O_n 's are the derivative operators acting on the external legs of the original graph, as carried over from Eq. (2.9). The time-dependent momenta entering the vertex factor G_n are given by

$$p_i^\mu(\eta) = \left(0, \frac{\mathbf{k}_i}{a(\eta)} \right) \quad (i = 1, \dots, n). \quad (2.21)$$

G_n is an amputated Feynman graph in flat-space, computed using the following Feynman rules:

1. For each vertex, insert a factor of $+i\lambda_a (a = 1, \dots, \mathcal{V})$.
2. Conserve the four-momentum at each vertex. This fixes the four-momentum \bar{q}_{bc}^μ , associated with the internal line connecting vertices b and c , in terms of the external four-momenta p_i^μ and loop momenta $\bar{q}_j^\mu (j = 1, \dots, \mathcal{L})$ (with \mathcal{L} denoting the number of loops). Notice that the total four-momentum of the graph is guaranteed to vanish because $\sum_{i=1}^n p_i^\mu = (0, \sum_{i=1}^n \mathbf{k}_i) = 0$.
3. Assign a Feynman propagator $\frac{-i}{\eta_{\mu\nu}(\bar{q}_{bc})^\mu (\bar{q}_{bc})^\nu + m^2 + i\epsilon}$ to each internal line.
4. For each loop, insert a factor of $\int \frac{d^4\bar{q}}{(2\pi)^4}$.
5. For each spacetime derivative $a^{-1}(\eta)\partial_\mu\sigma$ acting on the heavy field, insert a factor of $i(\bar{q}_{bc})_\mu$, where $\bar{q}_\mu = \eta_{\mu\nu}\bar{q}^\nu$.

Because G_n is an amputated diagram, derivatives acting on the external legs have no impact on its structure. Depending on the type of vertices, Lorentz indices appearing in G_n might be contracted with those appearing in O_n . We also emphasize that the external energies p_i^0 appearing in the flat-space graph G_n are identically set to zero, while ω_i 's have to be kept finite inside the bulk-to-boundary propagators $K^+(\omega_i, \eta)$ appearing in the integrand of the MFS reduction formula.

Before delving into the derivation of the MFS limit reduction formula, let us highlight a few key points. At first glance, one might expect that in the $m/H \rightarrow \infty$ limit, a heavy graph would reduce to a series of contact terms in an effective field theory. This EFT would result from integrating out the heavy field and would be expressed as an expansion in powers of ∇/m . However, this expectation does not hold due to the double-scaling nature of the MFS limit: As we increase m , we simultaneously send $\omega_i/k_i \rightarrow 0$, inversely proportional to m . This interplay implies that at the characteristic time $|\eta_c| \sim \mathcal{O}(1/\omega)$ (where ω represents the typical size of the external energies) the kinetic energy of the massive field becomes of the same order as its mass, specifically $|\mathbf{k}_i|/a(\eta_c) \sim \mathcal{O}(m)$. Therefore, around $\eta \sim \eta_c$, corresponding to the moment when the *physical* energies of the external legs ($= \omega_i/a(\eta)$) become comparable to the Hubble scale H^6 , it is not justified to expand in spatial derivatives. This shows that we are in a limit where the effective action is spatially *non-local*, a point we come back to in Section 2.4.

In the MFS limit, an important simplification arises in the structure of the propagators. As previously discussed, the in-in graph F_n includes contributions from all possible \pm vertex combinations in its original definition. However, in the heavy mass limit, terms associated with time-ordered or anti-time-ordered propagators dominate, while non-time-ordered contributions become exponentially suppressed in mass, hence negligible. At the level of the reduction formula (2.20), the all-plus contributions are captured by the G_n vertex factor, while all-minus terms appear in G_n^* .

Finally, we emphasize that the MFS limit also applies to loop diagrams, which can exhibit UV divergences requiring consistent regularization. In this work, we employ dimensional regularization to regulate the loop integrals in both the correlators (F_n) and their associated Feynman

⁶For linear dispersion relations, i.e., $\omega = c_s|\mathbf{k}|$, η_c corresponds to sound-horizon crossing.

graphs (G_n). When UV divergences are present, it is assumed that both sides of the the MFS limit reduction formula are expressed in d -dimensions (with $d \neq 4$). We will elaborate on this point further when discussing bubble graphs below.

Example: the single-exchange diagram. Let us inspect the MFS limit of a simple diagram, namely the tree-level exchange four-point function F_{SE} (Fig. 3), which is described by Eq. (2.12). The off-shell version of this diagram is simply obtained by setting $k_{12} \rightarrow \omega_{12}$ and $k_{34} \rightarrow \omega_{34}$, where $\omega_{ij} = \omega_i + \omega_j$.

The reduction formula implies that

$$F_{\text{SE}}(\omega_i, \mathbf{k}_i) \xrightarrow{\text{MFS}} -2 \text{Im} \int_{-\infty(1-i\epsilon)}^0 d\eta \frac{1}{s^2 \eta^2 + \frac{m^2}{H^2}} \exp(i\omega_T \eta). \quad (2.22)$$

The amputated diagram in this case is a single-exchange four-point function in flat-space, given by

$$G_4(p_i^\mu) = \frac{i}{\eta_{\mu\nu}(p_1 + p_2)^\mu (p_1 + p_2)^\nu + m^2 + i\epsilon} = \frac{i}{H^2 s^2 \eta^2 + m^2 + i\epsilon}, \quad (2.23)$$

in which

$$p_1 + p_2 = \left(0, \frac{\mathbf{k}_1 + \mathbf{k}_2}{a(\eta)} \right), \quad (2.24)$$

is the four-momentum exchanged in the s -channel of the flat-space graph.

For this specific graph, the time integral can be directly performed, leading to

$$F_{\text{SE}}^{\text{MFS}} = \frac{1}{s} \frac{H}{2m} \text{Re} \left\{ \exp\left(-\frac{\omega_T m}{s H}\right) \text{Ei}\left(\frac{\omega_T m}{s H} + i\epsilon\right) - \exp\left(\frac{\omega_T m}{s H}\right) \text{Ei}\left(-\frac{\omega_T m}{s H} + i\epsilon\right) \right\}, \quad (2.25)$$

where $\text{Ei}(z)$ is the Exponential Integral function.

This formula, clearly demonstrates that the limit cannot be replicated by the local quartic operator $\frac{g^2}{m^2} \phi^4$, which would result from integrating out the massive field at tree level. Such EFT operator generates a contact diagram that is given by $F_{\text{SE}} \propto \frac{g^2}{m^2} \frac{1}{\omega_T}$, which is distinct from the function above, which is a non-rational function of $\frac{\omega_T m}{s H}$ ($\sim \mathcal{O}(1)$). This mismatch highlights the inherently non-local nature of the MFS limit.

It is instructive to assess the accuracy of the MFS formula by comparing it with the exact analytical result available for this particular tree-level, off-shell diagram. This is given by Equation (4.34) of the reference [62], which was obtained by solving the bootstrap equations for the four-point function in unphysical configurations.

To simplify the comparison, we plot both the exact four-point function and the asymptotic MFS limit, using the following conventions. The exact four-point can be written as

$$F_{\text{SE}} = \frac{1}{s} \hat{F}_{\text{SE}}(r, r'; m), \quad (2.26)$$

where it is parametrized in terms of

$$r = \frac{\omega_{12}}{s}, \quad r' = \frac{\omega_{34}}{s}. \quad (2.27)$$

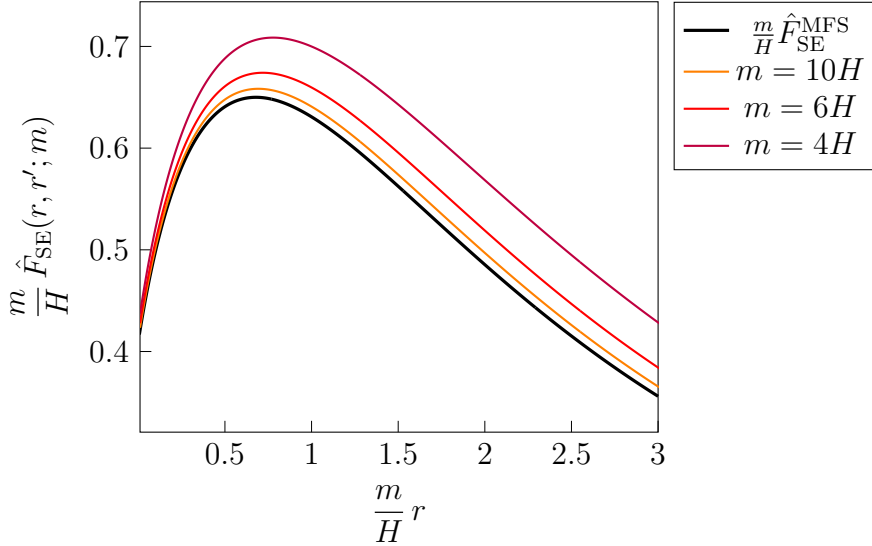


Figure 5: Comparison between the exact single-exchange diagram \hat{F}_{SE} with varying masses (the colored curves) and their massive flat-space limits $\hat{F}_{\text{SE}}^{\text{MFS}}$ (the black curve), all plotted as functions of $r \times (m/H)$ with a fixed value of $r' \times (m/H) = 0.2$.

In the MFS limit, $r \times (m/H)$ and $r' \times (m/H)$ are of order one. Therefore, it is reasonable to plot $\hat{F}_{\text{SE}}(r, r'; m)$ against $\hat{F}_{\text{SE}}^{\text{MFS}} \equiv s F_{\text{SE}}^{\text{MFS}}$ as a function of $\frac{m}{H}r$, while keeping $\frac{m}{H}r'$ fixed, as shown in Fig. 5.

The plot demonstrates excellent agreement between \hat{F}_{SE} and $\hat{F}_{\text{SE}}^{\text{MFS}}$ for large masses, confirming the validity of the MFS-limit approximation. Similar comparisons were made in [62], albeit with slightly different notations.

Comparison to the amplitude limit at $k_T = 0$. Finally, we compare our MFS limit to the conventional amplitude limit of correlators near their respective total energy singularity, $k_T = 0$ [10, 15, 19, 80, 81]. In this limit, the total energy singularity of a graph is proportional to the high-energy limit of the scattering process described by the same graph in flat space. This means that propagators' masses in the final amplitude go to zero.

Conversely, the propagators of the amputated flat-space Feynman graph appearing in (2.20) are massive. The difference arises because, in the ordinary flat-space limit, as $k_T \rightarrow 0$, the ratio m/H remains fixed. Sending $k_T \rightarrow 0$ has the effect of pushing all the vertices of the diagram to $-\infty$, where the kinetic energies of the internal lines grow indefinitely, rendering the masses comparatively negligible. In contrast, in the MFS limit, m is simultaneously sent to infinity, as ω_i 's approach zero, in an inversely proportional manner. As such, while by sending $\omega_i \rightarrow 0$, the vertices are sent to early times, the mass and the kinetic energies associated with the bulk-to-bulk propagators remain proportional.

Another key difference is that the amplitude limit captures only the leading-order behavior of the correlator near $k_T = 0$, whereas the MFS limit provides an approximation where the correlators are represented as smooth functions of the finite variable $\omega_i \times m/H$. In this way, the MFS limit contains infinitely more information than the amplitude limit, which isolates only the

singular component of the correlator.

2.3 From in-in integrals to the MFS limit

We now demonstrate how to formally derive the formula (2.20) by directly taking the MFS limit of the time integral representation of F_n , as given in Eq. (2.9). To make the discussion concrete, we focus on two specific examples: a single-exchange tree-level diagram and a one-loop bubble diagram. For simplicity, we assume the external legs correspond to massless or conformally coupled fields, but the derivation can be easily generalised to other fields in the complementary series.

The MFS limit of tree-level exchange diagrams

To analyze the asymptotic behavior of the heavy field's propagators in the large mass regime, we start with the free field equation of motion for σ in momentum space:

$$\eta^2 \partial_\eta^2 \sigma - 2\eta \partial_\eta \sigma + \left(s^2 \eta^2 + \frac{m^2}{H^2} \right) \sigma = 0. \quad (2.28)$$

For sufficiently large masses, this equation is amenable to a WKB approximation, which is valid from early times, $\eta \rightarrow -\infty$, all the way to the end of inflation, $\eta \rightarrow 0$. The solution can be expressed as:

$$\sigma_\pm^{\text{WKB}}(s, \eta) = \sum_\pm c_\pm(\eta_*) \frac{1}{a(\eta)} \left(s^2 + \frac{m^2}{H^2 \eta^2} \right)^{-1/4} \exp \left(\mp i \int_{\eta_*}^\eta d\eta' \sqrt{s^2 + \frac{m^2}{H^2 \eta'^2}} \right), \quad (2.29)$$

where η_* is an arbitrary integration constant that we choose to satisfy $|s\eta_*| \gg \frac{m}{H}$, without loss of generality. The coefficients c_\pm can be determined by matching the WKB solution to the Bunch-Davis vacuum at past infinity, where σ_+ behaves as

$$\lim_{\eta \rightarrow -\infty} \sigma_+(s, \eta) = -\frac{H\eta}{\sqrt{2s}} \exp(-is\eta). \quad (2.30)$$

This implies

$$c_+ \approx \frac{1}{\sqrt{2}} \exp(-is\eta_*), \quad c_- = 0. \quad (2.31)$$

It is important to note that the WKB solution in Eq. (2.29) does not account for particle production effects at late times. Such effects lead to a mixing of positive and negative frequency solutions, resulting in a small nonzero value for $c_- \propto e^{-\pi m/H}$. However, this contribution is exponentially suppressed in the heavy mass limit and can be safely neglected.

A single-exchange diagram. Now, consider a single-exchange diagram involving an arbitrary number of external conformally coupled fields (see Figure 6). In this case, the in-in expression

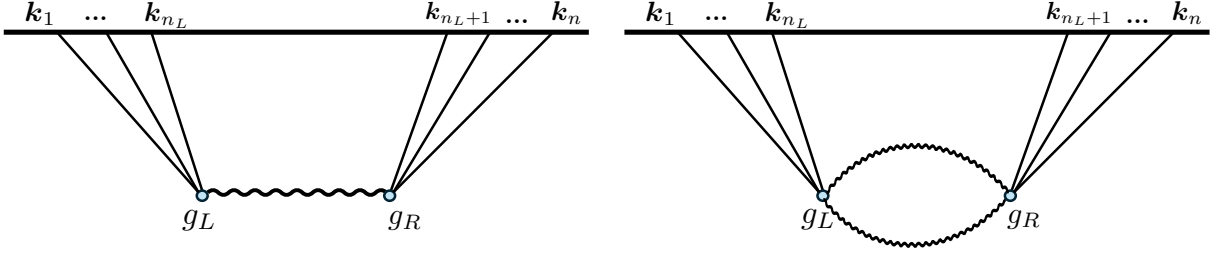


Figure 6: Generic single-exchange and one-loop, bubble graphs contributing to the n -point function of ϕ .

takes the following form:

$$\begin{aligned}
F_{\text{SE}}(\{\omega_i\}, \{\mathbf{k}_i\}; m) &= \sum_{\pm\pm} (\pm i g_L) (\pm i g_R) \int \frac{d\eta_1}{\eta_1^4 H^4} \frac{d\eta_2}{\eta_2^4 H^4} G_{\pm\pm}(s, \eta_1, \eta_2) \\
&\quad \left(\prod_{i=1}^{n_L} O_i(\eta_1, \partial_{\eta_1}, \mathbf{k}_i) K^\pm(\omega_i, \eta_1) \right) \left(\prod_{i=n_L+1}^n O_i(\eta_2, \partial_{\eta_2}, \mathbf{k}_i) K^\pm(\omega_i, \eta_2) \right) \\
&= \sum_{\pm\pm} (\pm i g_L) (\pm i g_R) \int d\eta_1 d\eta_2 f_{\pm\pm}(\eta_1, \eta_2) e^{\pm i \omega_L \eta_1} e^{\pm i \omega_R \eta_2} G_{\pm\pm}(s, \eta_1, \eta_2),
\end{aligned} \tag{2.32}$$

where $s = |\sum_{i=1}^{n_L} \mathbf{k}_i| = |\sum_{i=n_L+1}^n \mathbf{k}_i|$, g_L and g_R are the coupling constants at the left and right vertex, respectively. In the second line above, $f_{\pm\pm}$ is a polynomial in $\eta_{1,2}$ whose specific form is not important for the following argument, and we have defined $\omega_L = \sum_{i=1}^{n_L} \omega_i$ and $\omega_R = \sum_{i=1}^{n_R} \omega_{i+n_L}$, denoting the total external energy of the lines entering the left and right vertices, respectively, with $n_{L,R}$ denoting the number of external legs attached to each vertex.

It is useful to exchange $\eta_{1,2}$ for the following dimensionless variables

$$x_{1,2} = \frac{H}{m} s \eta_{1,2}, \tag{2.33}$$

and rewrite F_{SE} as

$$\begin{aligned}
F_{\text{SE}}(\{\omega_i\}, \{\mathbf{k}_i\}; m) &= \left(\frac{m}{H} \right)^2 \frac{1}{s^2} \sum_{\pm\pm} (\pm i g_L) (\pm i g_R) \times \\
&\quad \int_{-\infty(1 \mp i\epsilon)}^0 dx_1 dx_2 \tilde{f}_{\pm\pm}(x_1, x_2) \exp\left(\pm i \frac{m}{H} \frac{\omega_L}{s} x_1\right) \exp\left(\pm i \frac{m}{H} \frac{\omega_R}{s} x_2\right) G_{\pm\pm}\left(s, \frac{m}{H} x_1, \frac{m}{H} x_2\right),
\end{aligned} \tag{2.34}$$

where we have defined

$$\tilde{f}_{\pm\pm} = f_{\pm\pm} \left(\frac{m}{H} \frac{1}{s} x_1, \frac{m}{H} \frac{1}{s} x_2; s, \omega_i \right). \tag{2.35}$$

The above change of variable makes the highly oscillating parts of the integral manifest. Specifically, in the MFS limit, the first two exponential factors in Eq. (2.34) are slowly varying because

$$\frac{m}{H} \frac{\omega_R}{s} \sim \frac{m}{H} \frac{\omega_L}{s} \sim \mathcal{O}(1) \quad (\text{MFS limit}). \tag{2.36}$$

Using the solutions from (2.29) the bulk-to-bulk propagators are given by

$$\begin{aligned}
G_{\pm\pm} &= \frac{1}{2s^3} \left(\frac{m}{H}\right)^2 \frac{x_1}{(1+x_1^{-2})^{1/4}} \frac{x_2}{(1+x_2^{-2})^{1/4}} \exp\left(\mp i\frac{m}{H} \int_{x_1}^{x_2} dx' (1+\frac{1}{x'^2})^{1/2}\right) \theta(x_2 - x_1) \\
&\quad + x_1 \leftrightarrow x_2, \\
G_{\pm\mp} &= \frac{1}{2s^3} \left(\frac{m}{H}\right)^2 \frac{x_1}{(1+x_1^{-2})^{1/4}} \frac{x_2}{(1+x_2^{-2})^{1/4}} \exp\left(\pm i\frac{m}{H} \int_{x_1}^{x_2} dx' (1+\frac{1}{x'^2})^{1/2}\right). \tag{2.37}
\end{aligned}$$

Conversely to the first two exponential factors in (2.34), these propagators exhibit rapidly oscillating phases.

We first examine the $+-$ and $-+$ contributions to F_{SE} : The corresponding integrals over $\int dx_1 dx_2$ factorise, and each integral becomes exponentially small in the mass due to the fast oscillations of $G_{\pm\mp}$. This can be seen by noting that each integral takes the following schematic form

$$\mathcal{I}_{\pm} = \int_{-\infty(1\mp i\epsilon)}^0 dx \text{Poly}(x) \exp\left(\pm i\frac{m}{H} \frac{\omega}{s} x\right) \exp\left(\mp i\frac{m}{H} \int_{x_0}^x \frac{dx'}{x'} (1+x'^2)^{1/2}\right), \tag{2.38}$$

where x_0 is an arbitrary constant that drops out of $F_{\text{SE}}^{\pm\mp} (= \mathcal{I}_+ \times \mathcal{I}_-)$, and $\omega = \omega_L$ or ω_R . The second exponential factor above has the following convergent expansion around $x = 0$:

$$\begin{aligned}
&\exp\left(\pm i\frac{m}{H} \int_{x_*}^x \frac{dx'}{x'} (1+x'^2)^{1/2}\right) = \\
&(-x)^{\pm im/H} e^{\pm iC(x_0)} \left[1 \pm \frac{i}{4} \frac{m}{H} x^2 - \frac{1}{32} \left(\pm i\frac{m}{H} + \frac{m^2}{H^2}\right) x^4 + \dots\right], \tag{2.39}
\end{aligned}$$

where $C(x_0) = (1 - x_0 - \log(2)) m/H$, and $e^{\pm iC(x_0)}$ is a pure x -independent phase. Inserting this expansion in \mathcal{I}_{\pm} , we find

$$\mathcal{I}_{\pm} = \sum_n c_n^{\pm}(m) \int_{-\infty(1\mp i\epsilon)}^0 dx \text{Poly}(x) x^n \exp\left(\pm i\frac{m}{H} \frac{\omega}{s} x\right) (-x)^{\pm im/H} e^{\pm iC(x_0)}, \tag{2.40}$$

where $c_n^{\pm}(m)$ are the mass-dependent coefficients appearing within the bracket, in (2.39), which are polynomials in m/H . Sending mass to infinity causes all the terms above to vanish exponentially because they include a factor of the form

$$\int_{-\infty(1\mp i\epsilon)}^0 (-x)^{k\pm im/H} \exp\left(\mp i\frac{m}{H} \frac{\omega}{s} x\right) dx = \Gamma(1+k\mp im/H) \left(\pm i\frac{m}{H} \frac{\omega}{s}\right)^{-1-k\pm im/H} \quad (k \in \mathbb{Z}), \tag{2.41}$$

which is indeed exponentially small in the mass⁷.

In contrast, the $++$ and $--$ components receive non-negligible contributions from the vicinity of the diagonal $x_1 = x_2$. Within these blocks, at leading order in H/m , the propagators G_{++}

⁷A more direct method involves using the saddle point approximation to evaluate the integral 2.38. Due to the branch cut of the square root, it is somewhat nontrivial to show that the integral is indeed exponentially suppressed, which becomes evident after performing an appropriate contour deformation. We thank Yuhang Zhou for their correspondence on this point and refer the reader to [128] for details.

and G_{--} effectively resemble Dirac delta functions of the form $h(x_1, x_2)\delta(x_1 - x_2)$, where h is an appropriate multiplicative function. This behaviour becomes evident when the $\pm\pm$ propagators are expanded around the diagonal $x_1 = x_2$:

$$G_{\pm\pm} \sim \frac{1}{2s^3} \left(\frac{m}{H}\right)^2 \frac{x_1^3}{\sqrt{1+x_1^2}} \times \exp\left(\mp i\frac{m}{H}\left(1+\frac{1}{x_1^2}\right)^{1/2}\Delta x\right) (1 + \mathcal{O}(\Delta x)) \theta(\Delta x) + (\Delta x \rightarrow -\Delta x), \quad (2.42)$$

where $\Delta x = x_2 - x_1$. The $\pm\pm$ contributions take the following schematic form

$$\mathcal{F}_{\pm\pm} = \int_{-\infty(1\mp i\epsilon)}^0 dx \int_0^{\infty(1\pm i\epsilon)} d(\Delta x) (1 + \mathcal{O}(\Delta x)) J_{\pm}(x, \Delta x) \exp\left(\mp i\frac{m}{H}\left(1+\frac{1}{x^2}\right)^{1/2}\Delta x\right), \quad (2.43)$$

where J_{\pm} are slowly varying functions of x and Δx . In the $m/H \rightarrow \infty$ limit, this integral simplifies to:

$$\lim_{m \rightarrow \infty} \mathcal{F}_{\pm\pm} = \int_{-\infty(1\mp i\epsilon)}^0 dx \left(\pm i\frac{m}{H}\left(1+\frac{1}{x^2}\right)^{1/2}\right)^{-1} J_{\pm}(x, \Delta x = 0) (1 + \mathcal{O}(H/m)), \quad (2.44)$$

where the $\mathcal{O}(H/m)$ terms come from higher order corrections in Δx . The approximation above can be replicated by the following replacements:

$$G_{\pm\pm} \rightarrow \pm i\frac{1}{s^3} \frac{m}{H} \frac{x_1^3}{1+x_1^2} \delta(x_1 - x_2) = \pm i\frac{\eta^4}{\frac{m^2}{H^2} + s^2\eta^2} \delta(\eta - \eta'). \quad (2.45)$$

Note that both the $i\epsilon$ prescription and the step functions $\theta(\pm\Delta x)$ in the propagators were crucial to reaching this conclusion.

Using the asymptotic behavior of the $\pm\pm$ propagators derived above and ignoring the exponentially suppressed $\pm\mp$ branches, we ultimately recover the MFS limit of the single-exchange diagram. This corresponds to Eq. (2.20) with the following flat-space amputated n -point diagram:

$$G_n = g_L g_R \frac{i}{s^2/a^2(\eta) + m^2} = g_L g_R \frac{i}{(p_1(\eta) + \dots + p_{n_L}(\eta))^2 + m^2},$$

where $p_i^\mu(\eta) = (0, \mathbf{k}_i/a(\eta))$ are the fictitious, time-dependent four-momenta associated with the external legs.

The MFS limit of one-loop, bubble diagrams

Consider a one-loop bubble diagram, as depicted in Figure 6, and described by the following expression:

$$\begin{aligned}
F_{\text{Bubble}}(\{\omega_i\}, \{\mathbf{k}_i\}; m) &= \sum_{\pm\pm} (\pm i g_L)(\pm i g_R) \int \frac{d\eta_1}{(\eta_1 H)^d} \frac{d\eta_2}{(\eta_2 H)^d} \\
&\times \mu^{4-d} \int \frac{d^{d-1}\mathbf{q}}{(2\pi)^{d-1}} G_{\pm\pm}(|\mathbf{q}|, \eta_1, \eta_2) G_{\pm\pm}(|-\mathbf{q} + \mathbf{s}|, \eta_1, \eta_2) \\
&\times \left(\prod_{i=1}^{n_L} O_i(\eta_1, \partial_{\eta_1}, \mathbf{k}_i) K^\pm(\omega_i, \eta_1) \right) \left(\prod_{i=n_L+1}^n O_i(\eta_2, \partial_{\eta_2}, \mathbf{k}_i) K^\pm(\omega_i, \eta_2) \right). \tag{2.46}
\end{aligned}$$

The diagram is regulated using dimensional regularization [88, 93, 96, 129]. For consistency with dim. reg., the mode functions associated with both the external and internal lines have to be analytically continued to d dimensions, though in this case continuing the bulk-to-boundary propagators to general dimensions is inconsequential. Additionally, the renormalization scale μ is introduced to adjust the dimensionality of the loop integral.

In the heavy mass limit $m/H \rightarrow \infty$, similar to the tree-level case, the $+-$ and $-+$ contributions in the second line of Eq. (2.46) yield factorized terms (in η_1 and η_2), each of which is exponentially suppressed due to the rapid oscillations of $\sigma_\pm(q, \eta_{1,2})\sigma_\pm(|\mathbf{s} - \mathbf{q}|, \eta_{1,2})$. In contrast, using the approximate solutions from Eq. (2.29), the squares of the $++$ and $--$ propagators take the following form:

$$\begin{aligned}
G_{\pm\pm}(|\mathbf{q}|, \eta_1, \eta_2) G_{\pm\pm}(|\mathbf{s} - \mathbf{q}|, \eta_1, \eta_2) &= \frac{1}{2} H(\eta_1, \eta_2) \theta(\eta_2 - \eta_1) \\
&\times \exp\left(\mp i \int_{\eta_1}^{\eta_2} d\eta \left(\mathbf{q}^2 + \frac{m^2}{H^2 \eta^2}\right)^{1/2}\right) \exp\left(\mp i \int_{\eta_1}^{\eta_2} d\eta \left(|\mathbf{s} - \mathbf{q}|^2 + \frac{m^2}{H^2 \eta^2}\right)^{1/2}\right) + \eta_1 \leftrightarrow \eta_2, \tag{2.47}
\end{aligned}$$

where

$$\begin{aligned}
H(\eta_1, \eta_2) &= \frac{1}{2 a^{d-1}(\eta_1) a^{d-1}(\eta_2)} \left(q^2 + \frac{m^2}{H^2 \eta_1^2}\right)^{-1/4} \left(q^2 + \frac{m^2}{H^2 \eta_2^2}\right)^{-1/4} \\
&\times \left((\mathbf{s} - \mathbf{q})^2 + \frac{m^2}{H^2 \eta_1^2}\right)^{-1/4} \left((\mathbf{s} - \mathbf{q})^2 + \frac{m^2}{H^2 \eta_2^2}\right)^{-1/4}. \tag{2.48}
\end{aligned}$$

In analogy to the tree-level case, for a fixed \mathbf{q} , the rapid oscillations of the phases in the large-mass regime suppress the time integrals, except within a narrow region around the diagonal $\eta_1 = \eta_2$. Consequently, the squares of the propagators effectively behave like distributions that are proportional to $\delta(\eta_1 - \eta_2)$.

The coefficients of these Dirac delta distributions can be derived similarly to Eq. (2.49), re-

sulting in:

$$\begin{aligned}
& G_{\pm\pm}(|\mathbf{q}|, \eta_1, \eta_2) G_{\pm\pm}(|\mathbf{s} - \mathbf{q}|, \eta_1, \eta_2) \sim \\
& \pm i \left((q^2 + \frac{m^2}{H^2 \eta_1^2})^{1/2} + ((\mathbf{s} - \mathbf{q})^2 + \frac{m^2}{H^2 \eta_1^2})^{1/2} \right)^{-1} H(\eta_1, \eta_1) \delta(\eta_1 - \eta_2), \\
& = \pm i \frac{1}{2} (-H\eta_1)^{2d+1} \frac{1}{E_q(\eta_1) E_{|\mathbf{s}-\mathbf{q}|}(\eta_1)} \frac{1}{E_q(\eta_1) + E_{|\mathbf{s}-\mathbf{q}|}(\eta_1)} \delta(\eta_1 - \eta_2),
\end{aligned} \tag{2.49}$$

where in the last line we have introduced the time-dependent energy variables

$$E_k(\eta) = \left(\frac{k^2}{a^2(\eta)} + m^2 \right)^{1/2}. \tag{2.50}$$

We emphasize that the effectiveness of replacing $G_{\pm\pm}^2$ with a Dirac delta function remains unchanged as we vary the loop momentum. In fact, for ultraviolet modes, where $|\mathbf{q}| \rightarrow \infty$, this approximation improves further due to the phase factor in Eq. (2.47), which grow with $|\mathbf{q}|$.

We proceed with simplifying the expression in (2.49): The last line can be recast as an integral over a fictitious energy variable \bar{q}^0 , namely we can write:

$$\begin{aligned}
& \frac{1}{2} \frac{1}{E_q(\eta_1) E_{|\mathbf{s}-\mathbf{q}|}(\eta_1)} \frac{1}{E_q(\eta_1) + E_{|\mathbf{s}-\mathbf{q}|}(\eta_1)} = \\
& - \int_{-\infty}^{+\infty} \frac{d\bar{q}^0}{2\pi i} \frac{1}{-(\bar{q}^0)^2 + E_q^2(\eta_1) + i\epsilon} \frac{1}{-(\bar{q}^0)^2 + E_{|\mathbf{s}-\mathbf{q}|}^2(\eta_1) + i\epsilon}.
\end{aligned} \tag{2.51}$$

By combining \bar{q}^0 and \mathbf{q}/a , it is natural to form a full four-momentum in d dimension, namely

$$\bar{q}^\mu = (\bar{q}^0, \mathbf{q}/a(\eta)), \tag{2.52}$$

in terms of which the measure of the momentum integrals can be re-expressed as

$$d\bar{q}^0 d^{d-1} \mathbf{q} = d^d \bar{q} (H\eta)^{d-1}. \tag{2.53}$$

Using the new four-momentum \bar{q} we can rewrite the middle term in Eq. (2.46) as

$$\begin{aligned}
& \mu^{4-d} \int \frac{d^{d-1} \mathbf{q}}{(2\pi)^{d-1}} G_{\pm\pm}(|\mathbf{q}|, \eta_1, \eta_2) G_{\pm\pm}(|-\mathbf{q} + \mathbf{s}|, \eta_1, \eta_2) = \\
& \mp \mu^{4-d} (-\eta H)^d \int \frac{d^d \bar{q}}{(2\pi)^d} \frac{1}{\bar{q}^2 + m^2 + i\epsilon} \frac{1}{(\bar{q} - \bar{\mathbf{s}})^2 + m^2 + i\epsilon},
\end{aligned} \tag{2.54}$$

where we have introduced the artificial four-momentum

$$\bar{\mathbf{s}}^\mu = (0, \mathbf{s}/a(\eta)). \tag{2.55}$$

Substituting the simplified expression (2.56) in (2.46), we recover the MFS reduction formula for the one-loop diagram, with

$$G_n(p_1(\eta), \dots, p_n(\eta)) = (ig_L) (ig_R) \mu^{4-d} \int \frac{d^d \bar{q}}{(2\pi)^d} \frac{-i}{\bar{q}^2 + m^2 + i\epsilon} \frac{-i}{(\bar{q} - \sum_{i=1}^{n_L} p_i(\eta))^2 + m^2 + i\epsilon}. \tag{2.56}$$

As explained in Section 3.3, the UV divergent part of G_n , as $d \rightarrow 4$, must be canceled by an appropriate local counterterm in the action or, equivalently, by adding a contact diagram. We discuss this point further in Section 3.3.

In Appendix B, we provide an alternative proof of the MFS limit of the bubble diagram based on its spectral decomposition. Starting with the Källén–Lehmann representation of the composite operator σ^2 , we express the bubble diagram as an integral over an infinite continuum of tree-level exchange diagrams, each weighted by a spectral density [58]. In the heavy mass limit, $m \rightarrow \infty$, we show that the spectral density in this representation reduces to its Minkowski-space counterpart, with corrections suppressed by powers of H/m . The asymptotic behavior of the spectral density, combined with the reduction formula for the tree-level diagram (2.22), reproduces the expected MFS limit of the bubble graph.

2.4 The MFS limit from the effective action in curved spacetime

In this section, we derive the MFS limit reduction formula directly from the path integral by examining how the effective action arises after integrating out internal massive lines. The key insight is that when the Compton wavelength of a massive field in a curved background is much smaller than the characteristic scale set by the background curvature H , the field can be integrated out using an *in-out* path integral approach. This viewpoint is standard in much of the QFT literature on curved spacetime, where background curvature is treated perturbatively within the in-out effective action relative to other mass scales in the problem (see, e.g., [130]). Not surprisingly, this approach inherently overlooks non-perturbative effects, such as particle production due to curvature, which cannot be captured at any perturbative order in the in-out effective action.

As argued earlier, in the large-mass limit, the contributions from non-time-ordered propagators, which correspond to mixed terms connecting the upper and lower branches of the Schwinger-Keldysh contour, become exponentially small. This suppression arises from the rapid oscillatory behavior of the Wightman functions in the heavy-mass regime. Consequently, the dominant contributions to the effective action and resulting correlators are well-approximated by terms constructed solely from time-ordered propagators and their complex conjugates. Under these assumptions, the in-out path integral is adequate for computing the effective action, with interactions governed by time-ordered Feynman propagators, thereby simplifying the analysis.

The in-out effective action is expressed as:

$$e^{iS_{\text{eff}}(\phi)} = \int \mathcal{D}\sigma e^{iS(\phi, \sigma)}, \quad (2.57)$$

where σ is the heavy field, and ϕ denotes the light degrees of freedom. Typically, to compute correlation functions of $\phi(x)$ at sufficiently large separations, S_{eff} is expressed as a sum of local operators involving ϕ and its derivatives, organized by an increasing number of derivatives. However, as we will show below, in our case, the spatial derivatives are not small compared to the mass of σ . As a result, S_{eff} must be treated as a non-local effective action (see also [122, 131–133]).

We will divide the proof into two. First, we show that for very heavy fields, the Feynman propagator can be expressed in terms of the flat-space propagator up to curvature corrections

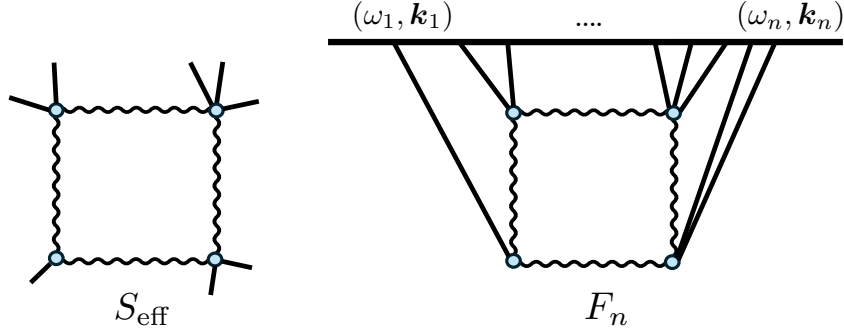


Figure 7: A sample amputated diagram contributing to the effective action of ϕ obtained by integrating out the heavy field, perturbatively. After dressing its external legs with bulk-to-boundary operators, the same diagram contributes to the n -point correlator of ϕ (in the notation of Eq. (2.58), here we have $n = 8$, $\mathcal{V} = r = 4$, $\mathcal{L} = 1$, $t_1 = 1$, $t_2 = t_4 = 2$ and $t_3 = 3$).

suppressed by powers of H/m . Second, we demonstrate that in the MFS limit, interaction vertices can be explicitly made local in time while maintaining non-locality in space.

Let us start by computing the Wilsonian in-out effective action. Since the fields ϕ and σ are weakly coupled, the path integral in Eq. (2.57) can be evaluated perturbatively. For simplicity, we focus on the case where all interaction vertices are polynomial and of the form $\phi^n \sigma^m$, without derivatives. Extending the proof to include derivative interactions is straightforward and does not alter the core arguments.

A connected Feynman diagram with n external legs and \mathcal{V} vertices, connected exclusively by heavy internal lines, contributes to the effective action a term of the schematic form:

$$iS_{\text{eff}} \supset \left(\prod_{a=1}^{\mathcal{V}} \int i\lambda_a \sqrt{-g(x_a)} d^d x_a \right) \left(\prod_{\text{internal lines (b,c)}} \Delta_F(x_b, x_c) \right) \phi^{t_1}(x_1) \phi^{t_2}(x_2) \dots \phi^{t_r}(x_r), \quad (2.58)$$

where $r \leq \mathcal{V}$ is the number of vertices attached to the external fields, λ_a 's are the coupling constants, $t_a (a = 1, \dots, r)$ is the number of external legs attached to the \mathcal{V} -th vertex (the total number of external legs is then $n = \sum_{i=1}^{\mathcal{V}} t_a$), and Δ_F is the Feynman propagator in curved space attributed to the scalar σ , namely

$$\Delta_F(x, x') = \langle \text{VAC} | T \{ \sigma(x) \sigma(x') \} | \text{VAC} \rangle. \quad (2.59)$$

We have also expressed the action in $d \neq 4$ to accommodate for potential UV divergences in the diagram, which will be regulated using dim-reg. Notice that the effective action in (2.58) is unitary as a result of having dropped the non-time-ordered contributions, such as those arising from $\pm \mp$ propagators.

Curvature expansion of the propagator. The Feynman propagator in curved space satisfies the following PDE:

$$(\square - m^2) \Delta_F(x, x') = \frac{i}{\sqrt{-g(x)}} \delta^4(x - x'). \quad (2.60)$$

When $m \gg H$, it is expected that the massive propagators mediating between two external light fields can be locally expanded in powers of the spacetime curvature. This is because, in the large mass limit, the Compton wavelength of the massive field becomes much smaller than the curvature scale set by the Hubble parameter H . To make this notion precise, we introduce Riemann normal coordinates ξ in a neighborhood around the point x' . In these coordinates, the metric near $x' = 0$ can be expressed as:

$$\bar{g}_{\mu\nu} = \eta_{\mu\nu} - \frac{1}{3}R_{\mu\alpha\nu\beta}(x')\xi^\alpha\xi^\beta + \mathcal{O}(\xi^3), \quad (2.61)$$

where $R_{\mu\alpha\nu\beta}(x')$ is the Riemann curvature tensor at x' and $\eta_{\mu\nu}$ is the flat-space Minkowski metric. We can use these coordinates around x' and express the propagator in a local momentum space, following the approach introduced by Bunch and Parker [134]⁸. In this coordinate system, the Feynman propagator satisfies the following equation:

$$\left[\eta^{\mu\nu} \partial_\mu \partial_\nu - (m^2 - R(x')/6) - \frac{1}{3} \eta^{\mu\nu} R_{\alpha\mu}(x') \xi^\alpha \partial_\nu + \dots \right] ((-\bar{g}(\xi))^{\frac{1}{4}} \Delta_F(\xi; x')) = i \delta^d(\xi). \quad (2.62)$$

In de Sitter spacetime, the Ricci tensor takes the form $R_{\mu\nu} = (d-1)H^2 g_{\mu\nu}$, and \bar{g} , the determinant of the metric in Riemann normal coordinates, is expanded as $-1 + \frac{1}{3}R_{\mu\nu}\xi^\mu\xi^\nu + \dots$. The terms represented by dots in the equation correspond to contributions involving three or more derivatives of the metric. Within the brackets, indices are raised and lowered using the flat-space metric $\eta_{\mu\nu}$. In de Sitter spacetime, curvature corrections scale as $\nabla^m R^n \sim \mathcal{O}(H^{m+2n})$, making $H|\xi|$ and H/m suitable small expansion parameters. Solving the propagator equation iteratively in curvature yields:

$$\begin{aligned} \Delta_F(\xi; x') &= -i(-\bar{g}(\xi))^{-\frac{1}{4}} \int \frac{d^d \bar{q}}{(2\pi)^d} \frac{1}{\bar{q}^2 + m^2 + i\epsilon} e^{i\bar{q}_\mu \xi^\mu} \left(1 + \frac{R(x')}{6} \frac{1}{\bar{q}^2 + m^2 + i\epsilon} + \dots \right) \\ &= \Delta_{\text{flat}}(\xi) \left[1 - \frac{1}{12} R_{\mu\nu} \xi^\mu \xi^\nu - \frac{d-2}{12} \frac{R}{m^2} - \frac{1}{12} \frac{R}{m^2} \frac{F'(\sqrt{-\xi^2}m)}{F(\sqrt{-\xi^2}m)} \sqrt{-\xi^2}m + \dots \right], \end{aligned} \quad (2.63)$$

where $\xi^2 = \eta_{\alpha\beta} \xi^\alpha \xi^\beta$, and F is defined through,

$$\Delta_{\text{flat}}(\xi) = -i m^{d-2} F(\sqrt{-\xi^2}m) = \int \frac{d^d \bar{q}}{(2\pi)^d} \frac{-i}{\bar{q}^2 + m^2 + i\epsilon} e^{i\bar{q}_\mu \xi^\mu}. \quad (2.64)$$

More explicitly, the function F takes the form

$$F = \left(i m \sqrt{-\xi^2} \right)^{(2-d)/4} K_{d/2-1}(i m \sqrt{-\xi^2}) \quad (2.65)$$

where $K_{d/2-1}$ is the modified Bessel function of the second kind. We have that F is of order one for $\xi \sim \mathcal{O}(1/m)$, while it behaves as $\exp(-m\sqrt{-\xi^2})$ at long distances, which is either exponentially damping or highly oscillating. This asymptotic behavior implies that, in the heavy

⁸The curvature expansion of the propagator in (2.66) can be derived by various other methods, including the heat-kernel formulation (see, e.g., [135] and references therein).

mass limit, the effective action S_{eff} receives its dominant contribution from regions where the physical distance between the vertices x_a is of order $1/m$ or smaller. Larger separations are exponentially suppressed, confirming that the interactions mediated by the heavy field are highly localized in space. In the large-mass limit, it is therefore valid to substitute the expansion (2.63) into the effective action. This is because the dominant contributions to S_{eff} arise from regions where $\xi \sim \mathcal{O}(1/m)$, much smaller than the spacetime curvature scale $1/H$ in de Sitter. At leading order in H/m , we retain only the leading term, which allows us to use the Minkowski space representation of the Feynmann propagator Δ_{flat} to further simplify the calculations.

If needed, curvature corrections can be included systematically by perturbatively adding higher-order terms from the expansion within the bracket in Eq. (2.63). In general, the Feynman propagator $\Delta_F(x, x')$ can be written as the flat-space Feynman propagator $\Delta^{\text{flat}}(\xi)$, plus curvature-dependent corrections:

$$\Delta_F(x, x') = \Delta_{\text{flat}}(\xi^\mu) \left(1 + \sum_{n+l-2k \geq 0} \nabla^{n+l-2k} R^k(x') m^{-n} \xi^l \Delta_{n,l,k}(m \xi^\mu) \right), \quad (2.66)$$

where R represents the components the Riemann tensor $R_{\mu\nu\alpha\beta}$ and its contractions, ∇ is the covariant derivative (with suppressed indices). $\Delta_{n,l,k}$ are functions of the dimensionless combination $m\xi^\mu$, generically of order one.

It will be useful to rewrite the leading-order term of (2.63) by expressing the Feynman propagator in a locally defined Fourier space. To do this, we first relate the Riemann normal coordinates ξ to the original coordinates (η, \mathbf{x}) . At leading order, the transformation is given by:

$$\begin{aligned} \eta - \eta' &= \frac{1}{a(\eta')} \left[\xi^0 - \frac{1}{2} H \xi^i \xi^i + \mathcal{O}(\xi^3) \right], \\ x^i - x'^i &= \frac{1}{a(\eta')} \left[\xi^i - H \xi^0 \xi^i + \mathcal{O}(\xi^3) \right]. \end{aligned} \quad (2.67)$$

Inverting this transformation and substituting it into (2.63), we obtain the following expression for the Feynman propagator:

$$\begin{aligned} \Delta_F(x, x') &= \int \frac{d^d \bar{q}}{(2\pi)^d} \frac{-i}{\bar{q}^2 + m^2 + i\epsilon} \exp(-i \bar{q}^0 a(\eta')(\eta - \eta') + i \bar{q}^i a(\eta')(x^i - x'^i)) [1 + \mathcal{O}(H\xi, H/m)] \\ &= \frac{1}{a^d(\eta')} \int \frac{d^d q}{(2\pi)^d} \frac{-i}{q^2/a^2(\eta') + m^2 + i\epsilon} \exp(-iq^0(\eta - \eta') + iq^i(x^i - x'^i)) [1 + \mathcal{O}(H\xi, H/m)], \end{aligned} \quad (2.68)$$

where the non-linear powers of η and \mathbf{x} appearing in the exponent $\exp(iq_\mu \xi^\mu)$ have been absorbed schematically into the $\mathcal{O}(H\xi, H/m)$ corrections, and $q = \bar{q} a(\eta')$ is the comoving four-momentum.

Correlators from the effective action. We will now derive the MFS limit using the effective action given in Eq. (2.58). As discussed earlier, the in-out effective action can be used to compute correlation functions, assuming that boundary terms are negligible in the MFS limit. This implies that the heavy graph introduced in Eq. (2.9) should match, in the MFS limit, with the diagram

constructed using the effective action (see Figure 7). The latter can be expressed as:

$$\begin{aligned}
F'_n \left(\omega_i, \mathbf{k}_i; \frac{m}{H} \right) &= 2 \operatorname{Re} \left(\prod_{a=1}^{\mathcal{V}} \int i \lambda_a a^d(\eta_a) d\eta_a d^d \mathbf{x}_a \right) \prod_{\text{internal lines (b,c)}} \Delta_F(\eta_b, \mathbf{x}_b; \eta_c, \mathbf{x}_c) \\
&\times \prod_{i=1}^{t_1} \tilde{K}^+(\omega_i - i\epsilon, \mathbf{k}_i; \eta_1, \mathbf{x}_1) \prod_{i=t_1+1}^{t_2+t_1} \tilde{K}^+(\omega_i - i\epsilon, \mathbf{k}_i; \eta_2, \mathbf{x}_2) \cdots \prod_{i=t_{r-1}+1}^n \tilde{K}^+(\omega_i - i\epsilon, \mathbf{k}_i; \eta_r, \mathbf{x}_r),
\end{aligned} \tag{2.69}$$

where we have defined $F'_n = F_n(2\pi)^3 \delta^3(\sum_{i=1}^n \mathbf{k}_i)$, and the objects \tilde{K}^+ are defined by the following positive-energy plane wave:

$$\tilde{K}^+(\omega, \mathbf{k}; \eta, \mathbf{x}) \equiv K^+(\omega, \eta) \exp(-i\mathbf{k} \cdot \mathbf{x}). \tag{2.70}$$

The $i\epsilon$ term inserted in the argument of the bulk-to-boundary propagators ensures the convergence of the integrals in the $\eta_a \rightarrow -\infty$ limit. Note that the formula above corresponds to only one permutation out of a total of $t_1! \dots t_r!$.

The derivation of the MFS limit begins by observing that the dominant contributions to the effective action and F_n arise from configurations where the vertices are closely spaced, as characterized by the conditions $a(\eta_1)(\eta_a - \eta_1) \lesssim \mathcal{O}(1)/m$ and $a(\eta_1)|\Delta \mathbf{x}_a| \lesssim \mathcal{O}(1)/m$. This proximity allows one to consider a local expansion of the bulk-to-boundary propagators, $\tilde{K}^+(\omega, \mathbf{k}; x)$, around a reference vertex $x_1 = (\eta_1, \mathbf{x}_1)$. For conformally coupled external fields, the propagators simplify to $\tilde{K}^+ \propto \eta \exp(i\omega\eta)$, and their expansion introduces an overall oscillatory factor $\exp(i\omega_T \eta_1)$ in the integrand. Consequently, the integral over η_1 is dominated by the region $|\eta_1| \lesssim \omega_T^{-1}$, while contributions from $|\eta_1| \gg \omega_T^{-1}$ are suppressed by the rapid oscillations regulated by the $i\epsilon$ -prescription.

Within this regime, it is important to distinguish the behavior of time and spatial derivative expansions. The time separation, $\Delta\eta_a = \eta_a - \eta_1$, can be treated perturbatively since $|\Delta\eta_a| \sim \mathcal{O}(1)/m$. This allows for a controlled expansion in time derivatives, with higher-order corrections suppressed by powers of H/m . On the other hand, spatial separations $\Delta \mathbf{x}_a = \mathbf{x}_a - \mathbf{x}_1$ cannot be expanded in $\mathbf{k} \cdot \Delta \mathbf{x}_a$ due to the scaling behavior $|\mathbf{k} \cdot \Delta \mathbf{x}_a| \sim \mathcal{O}(1)$ in the MFS limit. Specifically, for $a(\eta_1)\Delta \mathbf{x}_a \sim \mathcal{O}(1)/m$, the combination $\frac{H}{m} \frac{k}{\omega_T} \sim \mathcal{O}(1)$ becomes non-negligible. This precludes a spatial derivative expansion of the bulk-to-boundary propagators in terms of $\mathbf{k} \cdot \Delta \mathbf{x}_a$.

To address this, we use the MFS form of the propagators, as expressed in Eq. (2.68). The translation invariance of the propagators simplifies the spatial integrals over $\Delta \mathbf{x}_a$, ensuring momentum conservation at each vertex. After performing these integrals, the internal 3-momenta, \mathbf{q}_{bc} , are expressed as linear combinations of external and loop momenta. The time integrals over $\Delta\eta_a$ yield $\mathcal{V} - 1$ energy-conserving delta functions of the form $(2\pi)\delta(\sum_b q_{bc}^0)$, where the sum runs over the energies flowing into the vertex c . External legs do not contribute to these sums as their energies are effectively set to zero.

Corrections to the approximation $a(\eta_a) \approx a(\eta_1)$ in the propagators are suppressed by $\mathcal{O}(H/m)$. Expanding the scale factor as $a(\eta_a) = a(\eta_1)(1 + \mathcal{O}(\Delta\eta_a/\eta_1))$ and incorporating these terms into the propagator shows that higher-order corrections are negligible. This results in a further simplification of the integrand, ensuring that time-dependent effects beyond leading order do not

affect the dominant contribution in the MFS limit. Finally, integrating over the internal energy components q_{bc}^0 , except for \mathcal{L} undetermined loop energies q_j^0 , leads to the final form:

$$F_n^{\text{MFS}} = 2 \text{Re} \left\{ i^{\mathcal{V}} \lambda_1 \dots \lambda_{\mathcal{V}} \int_{-\infty}^0 a^d(\eta_1) d\eta_1 \left(\prod_{i=1}^n K(\omega_i - i\epsilon, \eta_1) \right) \right. \\ \left. \times \left(\frac{1}{(a^d(\eta_1))^L} \prod_{j=1}^L \frac{d^d q_j}{(2\pi)^d} \right) \prod_{\text{internal lines (b,c)}} \frac{-i}{-(q_{bc}^0/a(\eta_1))^2 + \mathbf{q}_{bc}^2/a^2(\eta_1) + m^2} \right\}, \quad (2.71)$$

This result matches the reduction formula for F_n^{MFS} given in Eq. (2.20), with the amputated flat-space diagram given by

$$G_n(p_i^\mu) = (i\lambda_1) \dots (i\lambda_{\mathcal{V}}) \left(\prod_{j=1}^L \frac{d^d \bar{q}_j}{(2\pi)^d} \right) \prod_{\text{internal lines (b,c)}} \frac{-i}{\bar{q}_{bc}^2 + m^2}, \quad (2.72)$$

where the 4-momenta associated with the external legs are defined as $p_i^\mu = (0, \mathbf{k}_i/a(\eta_1))$, the loop physical momenta are defined by $\bar{q}_j = q_j/a(\eta_1)$, and the internal lines physical four-momenta \bar{q}_{bc} ($= q_{bc}/a(\eta_1)$) are determined in terms of the p_i 's and \bar{q}_j 's through energy momentum conservation at each vertex.

Finally, we address the inclusion of derivative interactions. Adding derivatives to the external legs does not alter the validity of the proof outlined above. This is because the derivation primarily relied on two key elements: the flat-space limit of the heavy field two-point function and the observation that the dominant contributions to the in-in time integrals arise from the region $|\eta_a| \lesssim 1/\omega_T$. These properties remain unchanged when derivatives are applied to the external fields. Consequently, Eq. (2.71) continues to hold, with the modification that $\prod_{i=1}^n K$ should be replaced by $\prod_{i=1}^n O_n(\mathbf{k}_i, \partial_\eta) K(\omega_i, \eta)$, where O_n are the appropriate derivative operators acting on the external legs.

For the internal lines, the momentum representation of the propagator in Eq. (2.68) makes it clear that spatial derivatives introduce factors of $\pm i\mathbf{q}_i$. Specifically, a derivative $\partial/\partial\mathbf{x}$ acting on $\Delta_F(x, x')$ introduces a factor of $+i\mathbf{q}_i$, while a derivative $\partial/\partial\mathbf{x}'$ introduces $-i\mathbf{q}_i$. Similarly, a time derivative with respect to η introduces a factor of $i\eta^0$, and a derivative with respect to η' gives:

$$\partial_{\eta'} \Delta_F \approx \int \frac{d^d \bar{q}}{(2\pi)^d} \frac{-i}{\bar{q}^2 + m^2} \exp(-ia(\eta')\bar{q}^0 \Delta\eta + ia(\eta')\bar{\mathbf{q}} \cdot \Delta\mathbf{x}) (i\bar{q}^0 a(\eta') - i\bar{q}^0 a(\eta') \Delta\eta/\eta'). \quad (2.73)$$

The second term in the bracket arises from the derivative acting on the scale factor $a(\eta')$. However, it can be neglected in the MFS limit, where $|a(\eta')\Delta\eta| < \mathcal{O}(1)/m$. This ensures that the dominant contributions come from the first term.

In conclusion, each spacetime derivative with respect to x (or x') acting on the propagator $\Delta_F(x, x')$, which always appears in the scale-invariant combination $a^{-1}(\eta) \frac{\partial}{\partial x}$ (or $a^{-1}(\eta') \frac{\partial}{\partial x'}$), introduces an additional factor of $i(\bar{q}_{bc})^\mu$ or $-i(\bar{q}_{bc})^\mu$ in the final MFS reduction formula, Eq. (2.71).

2.5 Back to on-shell correlators with a reduced sound speed

To generalize the reduction formula (2.71) to on-shell diagrams—where the external energies ω_i and momenta \mathbf{k}_i are no longer independent but instead obey a specific dispersion relation—we

$$G_{\text{SB}}(p^2) = \frac{p^\mu}{\mathcal{O}_L[\pi]\sigma^2} \text{ (bubble loop) } \frac{p^\mu}{\sigma^2 \mathcal{O}_R[\pi]} \quad G_{\text{SE}}(p^2) = \frac{p^\mu}{\mathcal{O}_L[\pi]\sigma} \text{ (exchange) } \frac{p^\mu}{\sigma \mathcal{O}_R[\pi]}$$

Figure 8: The building blocks of the scalar exchange and scalar bubble diagrams contributing to the correlators of π .

consider massless fields propagating at a reduced speed while interacting with heavy fields. A notable example of this scenario arises in the EFT of inflation, where scalar fluctuations typically propagate at a subluminal sound speed.

The free field Lagrangian for such species is given by:

$$S_2 = \int a^3(t) dt d^3 \mathbf{x} \left(\frac{1}{2} \dot{\pi}_c^2 - \frac{1}{2} \frac{c_s^2}{a^2(t)} (\partial_i \pi_c)^2 \right) = \int a^2(\eta) d\eta d^3 \mathbf{x} \left(\frac{1}{2} \pi_c'^2 - \frac{1}{2} c_s^2 (\partial_i \pi_c)^2 \right),$$

where π_c denotes the canonically normalized phonon π appearing in the EFT of inflation. The mode function for π_c is given by

$$\pi_{c,\pm}(|\mathbf{k}|, \eta) = \frac{H}{\sqrt{2c_s k}} (1 \pm i c_s k) \exp(\mp i c_s k \eta), \quad (2.74)$$

We also denote the corresponding bulk-to-boundary propagator by K_π .

Although the action for π_c strongly breaks the de Sitter boost symmetries, it preserves the dilatation symmetry, under which $\pi_c(\eta, \mathbf{x}) \rightarrow \pi_c(\lambda\eta, \lambda\mathbf{x})$. In the next chapter, we review the systematic construction of the EFT for π and its coupling to matter fields, guided by the underlying symmetries. For simplicity, we assume that the free actions of the heavy matter fields remain de Sitter invariant, corresponding to unit sound speeds.

Within the on-shell correlators of π_c , the limit $c_s \rightarrow 0$ effectively mimics the behavior of setting $\omega_i \rightarrow 0$ in the off-shell correlators analyzed previously. This correspondence arises because the sound speed c_s directly controls the dispersion relation, tying the external energies and momenta. Consequently, in an alternative MFS limit defined by:

$$c_s \rightarrow 0, \quad m/H \rightarrow \infty, \quad \text{with} \quad \alpha = \frac{c_s m}{H} < \infty, \quad (2.75)$$

the on-shell correlators of π enjoy a similar simplification. In this limit, an arbitrary on-shell n -point function of π_c with heavy internal lines reduces to:

$$F_n^{\text{MFS}}(\{\mathbf{k}_i\}, \frac{c_s m}{H}; m) = 2 \text{Re} \int_{-\infty(1-i\epsilon)}^0 d\eta a^4(\eta) G_n[p_1^\mu(\eta), \dots, p_n^\mu(\eta); m] \prod_{i=1}^n O_n K_\pi^+(|\mathbf{k}_i|, \eta). \quad (2.76)$$

This expression closely resembles Eq.,(2.20), with a key distinction: each bulk-to-boundary propagator is now evaluated at the original momentum magnitude $|\mathbf{k}_i|$ instead of ω_i , which does not appear in the expression. The four-momentum p_i remains unchanged, retaining its definition as $p_i = (0, \mathbf{k}_i/a(\eta))$. Finally, introducing a sound speed for the external legs does not change the definition of G_n , which still represents the flat-space diagram obtained by amputating the

external legs.

Correlators of π from two-vertex, heavy graphs. We will be interested in simpler diagrams containing only two vertices (see Figure 9). In these diagrams, the corresponding amputated contribution depends solely on the momenta at one of the vertices, denoted by $p^\mu = \sum_{i=1}^{n_L} p_i^\mu = -\sum_{i=n_L+1}^n p_i^\mu$, and can be expressed as $G_n(p^2)$. Within the MFS limit, the effective action for the light field π corresponding to such diagrams takes the form:

$$S_{\text{eff}} = \int a^4(\eta) d\eta d^3\mathbf{x} \mathcal{O}_L[\pi(\eta, \mathbf{x})] i G_n(\nabla^2/a^2(\eta)) \mathcal{O}_R[\pi(\eta, \mathbf{x})]. \quad (2.77)$$

where $\mathcal{O}_{L,R}$ are operators at the left and right vertices that couple to the heavy sector. These operators typically take the schematic form $\partial^\# \pi^{n_{L,R}}$, with $n_{L,R}$ being the number of external legs attached to each vertex. We emphasize again that G_n is generically non-analytic in p^2 , and therefore the above action is inherently *non-local* in space, even though it remains local in time.

Among all possible types of vertices, we will be especially interested in the following menu:

$$\begin{array}{ll} \mathcal{O}_{L,R}[\pi(x)]\sigma & \text{scalar single-exchange (SE)}, \\ \mathcal{O}_{L,R}[\pi(x)]\sigma^2 & \text{scalar bubble (SB)}, \end{array}$$

using which we can form single-exchange and one-loop, bubble graphs with external π legs (Figure 8). The corresponding amputated diagrams for these cases are given by:

$$\begin{aligned} G_{\text{SE}}(p^2) &= \frac{i}{p^2 + m^2}, \quad (2.78) \\ G_{\text{SB}}(p^2) &= \mu^{4-d} \int \frac{d^4\bar{q}}{(2\pi)^4} \frac{1}{\bar{q}^2 + m^2 + i\epsilon} \frac{1}{(\bar{q} - p)^2 + m^2 + i\epsilon} \\ &= \frac{i \mu^{4-d}}{(4\pi)^{d/2}} \Gamma(2 - d/2) \int_0^1 dx (m^2 + p^2 x(1-x))^{d/2-2} \\ &\rightarrow \frac{i}{16\pi^2} \int_0^1 dx \log \left[\frac{m^2 + x(1-x)p^2}{\mu^2} \right] + \frac{i}{8\pi^2} \left(-\frac{1}{(d-4)} + \frac{1}{2} \log(4\pi e^{-\gamma_E}) \right). \quad (2.79) \end{aligned}$$

We will use the $\overline{\text{MS}}$ scheme to regularize the bubble graphs, for which we will add counter terms of the form $\mathcal{O}_L[\pi]\mathcal{O}_R[\pi]$ to cancel the second term in the last line.

Finally, we discuss how to extend the effective action beyond the leading-order massive limit. The full effective action is expected to have the following form

$$S_{\text{eff}} = \int a^4(\eta) d\eta d^3\mathbf{x} \mathcal{O}_L[\pi(\eta, \mathbf{x})] i \tilde{G}_n(\square) \mathcal{O}_R[\pi(\eta, \mathbf{x})], \quad (2.80)$$

in which the D'Alembertian operator should be understood as

$$\square = \frac{1}{a^2(\eta)} \nabla^2 + \hat{\delta}, \quad \text{where } \hat{\delta} = \eta^2 \partial_\eta^2 - 2\eta \partial_\eta, \quad (2.81)$$

and the operator $\hat{\delta}$, which includes time derivatives, is to be treated perturbatively. For the single-exchange diagram (where $G_n \propto (p^2 + m^2)^{-1}$), we simply have $\tilde{G}_n = G_n$. In Appendix A, we show

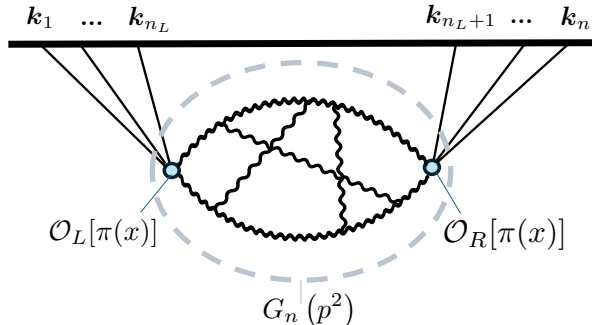


Figure 9: Two vertex, heavy graphs contributing to n -point correlators of phonons π .

that in this case, organizing G_n as a systematic expansion in $\frac{H}{m}\hat{\delta}$ corresponds to adding higher time-derivative corrections to the lowest-order non-local effective action in (2.77), see [62, 69]. At loop level, we generally expect $\tilde{G}_n \neq G_n$ due to the presence of curvature terms in the effective action, in addition to the terms arising from the flat-space limit by replacing ordinary derivatives with covariant ones. Computing these higher-order corrections requires accounting for sub-leading contributions in the propagator expansion, as well as previously neglected higher-order terms in Δx_a and $\Delta \eta_a$, which we leave for future work⁹.

3 Cosmological Phonon Collider

In this section, we apply the MFS reduction formula to compute sample tree-level and one-loop contributions to the bispectrum of curvature perturbations. These diagrams involve the exchange of heavy fields, which can be as massive as $H/c_s \gg H$, yet they leave imprints that cannot be captured by any local single-field theory for inflation.

3.1 EFT of inflation and energy scales

Single clock inflation can be thought of as a state of matter in which time translation symmetry is spontaneously broken. From this perspective, the long-wavelength scalar fluctuation during inflation manifests itself as the Goldstone mode that non-linearly realizes the broken time translation. More specifically, under an arbitrary time diffeomorphism $t \rightarrow t - \xi$, the Goldstone field $\pi(t, \mathbf{x})$ transforms as $\pi \rightarrow \pi(t - \xi, \mathbf{x}) + \xi$. In order to construct an effective field for the fluctuations, it is convenient to start from the unitary gauge, defined by $\pi = 0$. In this gauge, the EFT should be invariant only under the action of spatial diffs. As a result, at leading order in derivatives, the EFT building blocks comprise g^{00} , the extrinsic curvature of constant time hypersurfaces $K_{\mu\nu}$ along with fully covariant quantities constructed out of the Riemann tensor. The action then

⁹Alternatively, the one-loop effective action can be computed using the Schwinger-De Witt asymptotic expansion, which facilitates the inclusion of curvature corrections; see, e.g., [136].

takes the following form:

$$S = \int d^4x \sqrt{-g} \left(\frac{1}{2} M_P^2 R + M_P^2 \dot{H} g^{00} - M_P^2 (3H^2 + \dot{H}) + \frac{1}{2} M_2^4 \delta g_{00}^2 + \frac{1}{2} M_3^4 \delta g_{00}^3 + \dots - \frac{1}{2} \bar{M}_2^4 \delta K_\mu^{\mu 2} + \dots \right), \quad (3.1)$$

where, using the background equation of motion, the Lagrangian has been fixed up to terms that are quadratic or higher in perturbations, namely in $\delta g_{00} = 1 + g_{00}$ and $\delta K_{\mu\nu} = K_{\mu\nu} - a^2 h_{\mu\nu}$ (with $h_{\mu\nu}$ standing for the induced metric on the constant time hypersurfaces). To leading order in slow-roll parameters, the model-dependent coefficients M_i and \bar{M}_i can be taken as time independent constants.

The full four-dimensional covariance of the action (3.1) can be restored via the Stueckelberg trick, namely by sending $t \rightarrow t - \pi(t, \mathbf{x})$. We will be interested in the so called decoupling limit of the system, where we take

$$M_{\text{Pl}} \rightarrow \infty, \quad |\dot{H}| \rightarrow 0 \quad (M_{\text{Pl}}^2 |\dot{H}| = \text{fixed}). \quad (3.2)$$

In this limit, the π sector decouples from metric perturbations, and the action for scalar perturbations simplifies to

$$S_\pi = \int dt d^3x a^3 \frac{M_{\text{Pl}}^2 |\dot{H}|}{c_s^2} \left[\dot{\pi}^2 - c_s^2 (\tilde{\partial}_i \pi)^2 + (1 - c_s^2) \left(\dot{\pi} (\tilde{\partial}_i \pi)^2 + \frac{A}{c_s} \dot{\pi}^3 \right) + \dots \right], \quad (3.3)$$

where $\tilde{\partial}_i = a^{-1} \partial_i$, and dots stand for terms with higher derivatives or powers of π . Most notable in this Lagrangian is the universal cubic operator $\dot{\pi} (\partial_i \pi)^2$ with its coefficient uniquely fixed by the speed of sound c_s , as opposed to the competing cubic interaction $\dot{\pi}^3$ with an independent coefficient. We also highlight the fact that, in the decoupling limit, single-clock inflation exhibits the same symmetry breaking pattern as a superfluid condensate at zero temperature. Therefore, the same effective field theory as (3.3) applies to the dynamics of superfluid's *phonons* (see, e.g., [137–140]).

We are interested in additional weakly coupled relativistic fields during inflation (with unit sound speeds). In addition to the Hubble scale, there are four relevant energy scales in our setup:

- The symmetry breaking scale $f_\pi = (2c_s M_{\text{Pl}}^2 |\dot{H}|)^{1/4}$ associated with the broken time translation.
- The strong coupling scale of the EFT, given by

$$\Lambda_* = \left(\frac{24\pi}{5} \right)^{\frac{1}{4}} \frac{c_s}{(1 - c_s^2)^{\frac{1}{4}}} f_\pi, \quad (3.4)$$

above which the δg_{00}^2 operator in (3.1) becomes strongly coupled¹⁰.

¹⁰After performing the Stueckelberg trick, the operator δg_{00}^2 transforms to $(1 + \partial_\mu(t + \pi) \partial^\mu(t + \pi))^2 = (2\dot{\pi} + (\partial_\mu \pi)^2)^2$. It turns out that, within this block, the most conservative value for Λ_* follows from the perturbative unitarity of the $(\partial_i \pi)^4$ operator.

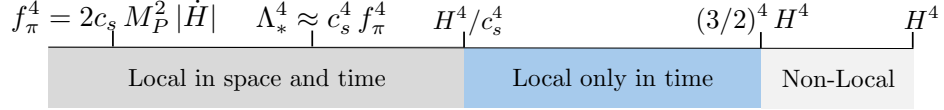


Figure 10: Characteristic energy scales in the EFT of inflation. Integrating out an additional heavy scalar results in an effective action for π , which is *non-local* in space but local in time, if $m < \mathcal{O}(1)H/c_s$, or local in both space and time when the field is heavier. Integrating out fields in the complementary series always gives fully non-local effective actions.

- H/c_s , namely the gradient energy of a relativistic field when its momentum crosses the sound horizon, i.e. $k/a = H/c_s$.
- The mass of the new particle m .

The symmetry breaking scale f_π is tied to the amplitude of the scalar powerspectrum ($\Delta_\zeta \sim 2.2 \times 10^{-9}$ [141]), namely we have $f_\pi = (2\pi\Delta_\zeta)^{-\frac{1}{2}}H \approx 58H$. The strong coupling scale Λ_* is bounded from below because of the Planck lower limit on the speed of sound (coming from Planck’s constraints on equilateral and orthogonal non-Gaussianity [142]):

$$c_s \geq 0.021 \text{ (95\%CL)} \quad \Rightarrow \quad \Lambda_* \gtrsim 2.3H. \quad (3.5)$$

We are interested in the correlators of the phonon π induced by the exchange of heavy fields in the MFS limit, namely

$$H \ll m \lesssim \mathcal{O}(1)H/c_s. \quad (3.6)$$

Integrating out heavy fields within this mass window yields an effective action for π that is generally nonlocal in space but remains local in time. For two-vertex heavy graphs, the corresponding Lagrangian takes the schematic form shown in Eq. (2.77). In contrast, integrating out heavier species produces the usual local higher-derivative operators in the EFT of inflation, while lighter particles result in fully non-local actions. While it is intriguing to describe the exchange of moderately heavy fields by adding new non-local operators to the EFT of inflation, it is not obvious how to construct a non-local EFT of inflation from a bottom-up point of view. Therefore, in all computations below, we rely on some known, local and weakly coupled UV framework. Finally, for the full consistency of our setup, we further require that the mass of the heavy field is below the cut-off of the EFT, i.e.,

$$m < \Lambda_*. \quad (3.7)$$

Depending on the value of c_s , this condition might be more stringent than the upper bound in Eq. (3.6).

3.2 Coupling matter fields to the EFT of inflation

It is straightforward to couple additional matter fields to the EFT of inflation. In this work, we focus on relativistic species that belong to the unitary representations of the de Sitter (dS) isometry

group $\text{SO}(4, 1)$. While the quadratic Lagrangian for these matter fields preserves dS isometries, we allow their interactions with the π sector to weakly break de Sitter boost invariance¹¹. Due to the weakly broken boosts, the π -correlators mediated by the exchange of these fields do not satisfy conformal Ward identities. Nevertheless, they continue to exhibit scale invariance.

In this work, we do not aim to construct the most general set of interactions between the matter fields and π . Instead, we focus on representative mixing terms that generate both tree-level and loop-level contributions to the π bispectrum. The computational techniques we develop to evaluate these diagrams are broadly applicable and can be easily adapted to incorporate other variations of the interaction vertices.

In the unitary gauge, we consider the following operators (up to quadratic order in the massive field):

$$(\delta g^{00})^n \sigma, (\delta g^{00})^n \sigma^2, \quad (3.8)$$

where $n = (1, 2)$. The first operator generates tree-level processes, while the second one contributes at loop level. Notably, for charged scalars, such as a Higgs-like field in the unbroken phase, the linear term is absent and their effect on π 's correlators start at one-loop level.

We employ the Stückelberg trick to reintroduce π , implemented through the transformation:

$$\delta g^{00} \rightarrow 1 + \bar{g}^{\mu\nu} \partial_\mu(t + \pi) \partial_\nu(t + \pi). \quad (3.9)$$

Substituting this into the action and taking the decoupling limit, we obtain the following set of interaction operators:

$$\begin{aligned} S_{\text{int}} &= \int d\eta d^3x a^4 \left(\mathcal{L}^{\sigma^1} + \mathcal{L}^{\sigma^2} \right), \quad (3.10) \\ \mathcal{L}^{(\sigma^1)} &= \rho \frac{1}{a(\eta)} \pi'_c \sigma + \frac{1}{\Lambda_1} \frac{1}{a^2(\eta)} \pi_c'^2 \sigma + \frac{1}{\bar{\Lambda}_1} \left(\frac{1}{a} \partial_i \pi_c \right)^2 \sigma + \dots, \\ \mathcal{L}^{(\sigma^2)} &= g \frac{1}{a(\eta)} \pi'_c \sigma^2 + \frac{1}{\Lambda_2} \frac{1}{a^2(\eta)} \pi_c'^2 \sigma^2 + \frac{1}{\bar{\Lambda}_2} \left(\frac{1}{a} \partial_i \pi_c \right)^2 \sigma^2 + \dots \end{aligned}$$

Here, we have retained only the terms that contribute to tree-level and one-loop diagrams of the π three-point function. The Lagrangian above is expressed in terms of the canonically normalized field $\pi_c = c_s^{-\frac{3}{2}} f_\pi^2 \pi$. The coupling constants ρ, g and $\Lambda_{1,2}$ are free parameters. However, due to the non-linearly realised boosts, the other scales $\bar{\Lambda}_{1,2}$ will be automatically dictated by the following relations:

$$\bar{\Lambda}_1 \rho = (\bar{\Lambda}_2)^2 g = -2f_\pi^2 c_s^{-\frac{3}{2}}. \quad (3.11)$$

¹¹Effective field theories can also be constructed for species that strongly break dS boosts at the level of the quadratic action. For massive scalars, this involves introducing a non-trivial speed of propagation, while for spinning fields, such breaking results in qualitatively different dynamics compared to their dS-symmetric counterparts; see, e.g., [143].

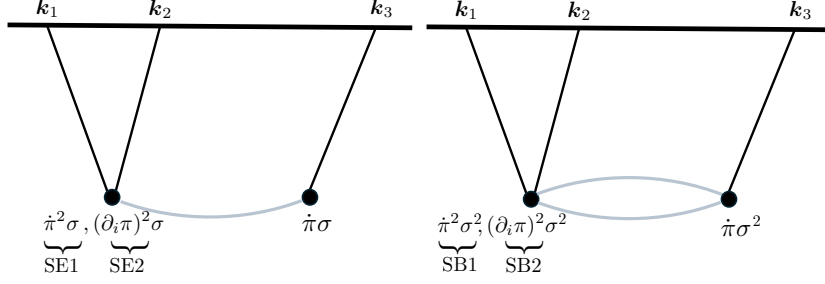


Figure 11: The tree-level and one-loop bubble contributions to the bispectrum, see Eq. (3.12).

In the notation of Eq. (2.77), we can form two scalar-exchange diagrams (hereafter SE1 and SE2) as well as two scalar-bubble diagrams (SB1 and SB2) by setting

$$\begin{aligned}
 & \left(\frac{1}{\Lambda_1 a^2(\eta)} \pi_c'^2, \frac{\rho}{a(\eta)} \pi_c' \right) \quad (\text{SE1}), & \left(\frac{1}{\Lambda_1} \left(\frac{1}{a} \partial_i \pi_c \right)^2, \frac{\rho}{a(\eta)} \pi_c' \right) \quad (\text{SE2}), \\
 & \left(\frac{1}{\Lambda_2 a^2(\eta)} \pi_c'^2, \frac{g}{a(\eta)} \pi_c' \right) \quad (\text{SB1}), & \left(\frac{1}{\Lambda_2} \left(\frac{1}{a} \partial_i \pi_c \right)^2, \frac{g}{a(\eta)} \pi_c' \right) \quad (\text{SB2}).
 \end{aligned} \tag{3.12}$$

where the components in each case corresponds to $\mathcal{O}_L[\pi]$ and $\mathcal{O}_R[\pi]$.

Unitarity bounds on the couplings. We work in the weak coupling regime, where the quadratic mixing term $\dot{\pi}\sigma$ can be treated perturbatively. This assumption imposes an upper bound on ρ :

$$\rho \lesssim m, \tag{3.13}$$

This bound can be inferred by assuming that the single-exchange diagrams correcting the propagators of π and/or σ remain small at energy scales of order $\omega_\pi \sim H$ [69, 144].

The other free energy scales are constrained by perturbative unitarity (see [69, 144])¹². For a rough estimation of the lower bounds on these scales, we neglect the mass of σ . The bound on the $\dot{\pi}^2\sigma$ operator can be estimated by comparing the one-loop and tree-level contributions to the three-point amplitude $\mathcal{A}_{2\pi \rightarrow \sigma}$ at energy scales of order the Hubble scale. Requiring the one-loop correction to be small relative to the contact term amplitude yields:

$$H/\Lambda_1 \ll 2\pi c_s. \tag{3.14}$$

Similarly, requiring the one-loop correction to $\mathcal{A}_{\pi \rightarrow 2\sigma}$ to remain subdominant compared to the $\dot{\pi}^2\sigma$ contact term gives:

$$g \ll 2\pi, \tag{3.15}$$

and, finally, perturbative unitarity of the $\mathcal{A}_{2\pi \rightarrow 2\sigma}$ amplitude imposes an upper bound on the size of the $\pi'^2\sigma^2$ operator:

$$H/\Lambda_2 \ll 2\pi c_s^{1/2}. \tag{3.16}$$

¹²A more rigorous approach to establishing perturbativity bounds on EFT coefficients involves studying the partial wave expansion of phonon amplitudes, as discussed in [145].

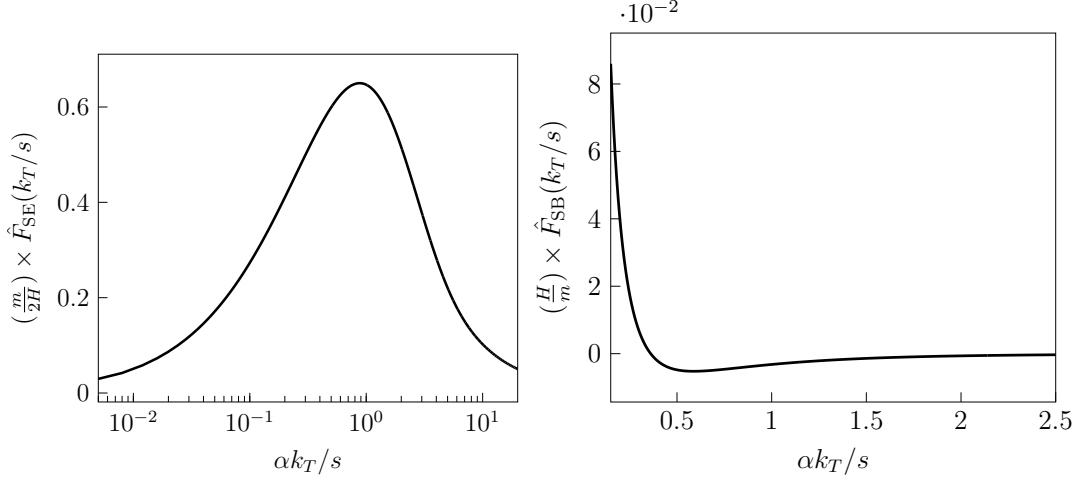


Figure 12: Plots of the tree-level and one-loop four-point functions of the conformally coupled field, scaled by the exchanged momentum s , i.e., $\hat{F}_{\text{SE,SB}} \equiv s \times F_{\text{SE,SB}}$.

Similar bounds can be placed on the energy scales $\bar{\Lambda}_{1,2}$, but they are weaker than bounds derived from Eq. (3.11).

3.3 Seed correlators from Mellin transformation

Weight-shifting operators. It is easy to show that all the four diagrams of our interest in (3.12) can be extracted from the off-shell four-point functions of the conformally coupled field, namely F_{SE} and F_{SB} , as defined in Eq. (2.12) and (2.13), respectively. These diagrams are extracted using a set of Weight-Shifting (WS) operators, which convert the external propagators of the conformally coupled fields into massless propagators with the requisite derivative structures. The derivation of the WS operators is detailed in [62]; here, we simply present the final result:

$$\begin{aligned}
\langle \pi_c(\mathbf{k}_1) \pi_c(\mathbf{k}_2) \pi_c(\mathbf{k}_3) \rangle'_{\text{SE1}} &= \frac{\rho}{H^3 \Lambda_1} \left(\prod_{i=1}^3 |\pi_c(k_i, \eta_0)|^2 \right) \hat{\mathcal{W}}_1(k_i, \frac{\partial}{\partial k_i}) F_{\text{SE}}(c_s k_i, s)|_{k_4 \rightarrow 0} \\
\langle \pi_c(\mathbf{k}_1) \pi_c(\mathbf{k}_2) \pi_c(\mathbf{k}_3) \rangle'_{\text{SB1}} &= \frac{g}{H \Lambda_2^2} \left(\prod_{i=1}^3 |\pi_c(k_i, \eta_0)|^2 \right) \hat{\mathcal{W}}_1(k_i, \frac{\partial}{\partial k_i}) F_{\text{SB}}(c_s k_i, s)|_{k_4 \rightarrow 0} \\
\langle \pi_c(\mathbf{k}_1) \pi_c(\mathbf{k}_2) \pi_c(\mathbf{k}_3) \rangle'_{\text{SE2}} &= \frac{\rho}{H^3 \Lambda_1} \left(\prod_{i=1}^3 |\pi_c(k_i, \eta_0)|^2 \right) \hat{\mathcal{W}}_2(k_i, \frac{\partial}{\partial k_i}) F_{\text{SE}}(c_s k_i, s)|_{k_4 \rightarrow 0} \\
\langle \pi_c(\mathbf{k}_1) \pi_c(\mathbf{k}_2) \pi_c(\mathbf{k}_3) \rangle'_{\text{SB2}} &= \frac{g}{H \Lambda_2^2} \left(\prod_{i=1}^3 |\pi_c(k_i, \eta_0)|^2 \right) \hat{\mathcal{W}}_2(k_i, \frac{\partial}{\partial k_i}) F_{\text{SB}}(c_s k_i, s)|_{k_4 \rightarrow 0}, \quad (3.17)
\end{aligned}$$

where

$$\begin{aligned}
\hat{\mathcal{W}}_1 &= -c_s^4 (k_1 k_2 k_3)^2 \frac{\partial^2}{\partial k_{12}^2}, \\
\hat{\mathcal{W}}_2 &= c_s^2 (\mathbf{k}_1 \cdot \mathbf{k}_2) k_3^2 \left(1 - k_{12} \frac{\partial}{\partial k_{12}} + k_1 k_2 \frac{\partial^2}{\partial k_{12}^2} \right). \quad (3.18)
\end{aligned}$$

On the RHS of the equations above, in the argument of the off-shell four-points $F_{\text{SE,SB}}$, we have set $\omega_i = c_s k_i (i = 1, 2, 3)$ and have taken the soft limit $k_4 \rightarrow 0$. Therefore, by conservation of momentum, we have $s = |\mathbf{k}_1 + \mathbf{k}_2| \rightarrow k_3$. Notice that the intermediate momentum s is not rescaled with the speed of sound, which reflects the fact that the exchanged fields have unit sound speeds.

As shown in the equations above, the same WS operator $\hat{\mathcal{W}}_{1,2}$ generates the SE1/2 and SB1/2 diagrams from their respective tree-level and one-loop seeds. This is due to the identical derivative structure in the external legs of these diagrams. It is also important to note that the equations above include only one permutation in each channel, and thus the result is not manifestly symmetric under permutations of k_1, k_2 and k_3 . The full three-point function, however, is obtained by summing over all permutations and all channels, hence fully permutation symmetric.

Seed correlators in the MFS limit. Having established the relationship between the π three-point function and the four-point functions of the conformally coupled field, the remaining task is to compute the latter seed correlators. In the MFS limit, these are given by

$$F_{\text{SE,SB}}(\omega_T, s) = 2 \operatorname{Re} \int_{-\infty(1-i\epsilon)}^0 d\eta G_{\text{SE,SB}}(s^2/a^2(\eta)) \exp(i\omega_T \eta), \quad (3.19)$$

where $G_{\text{SE,SB}}$ are given by Eq. (2.78). As discussed earlier, we use the $\overline{\text{MS}}$ scheme to regulate the loop diagram. In more detail, the second term in the last line of Eq. (2.79) contributes as

$$F_{\text{SB}} \supset \frac{1}{4\pi^2} \left(-\frac{1}{(d-4)} + \frac{1}{2} \log(4\pi e^{-\gamma_E}) \right) \frac{1}{\omega_T}, \quad (3.20)$$

which can be canceled by adding a ϕ^4 counter term to the action of the conformally coupled field. From this point forward, we assume that this subtraction has been performed, and G_{SB} denotes the remaining finite part of the loop graph, namely the first term in Eq. (2.79).

In the context of the π three-point function, the corresponding counterterms are $\dot{\pi}^3$ for the SB1 diagram and $\dot{\pi}(\partial_i \pi)^2$ for the SB2 diagram. The operator $\dot{\pi}\sigma^2$ also induces a one-loop contribution to the two-point function of π , resulting in a divergence that must be canceled by a quadratic counterterm of the form $\dot{\pi}^2$. This quadratic operator effectively modifies the speed of sound, ensuring that the coefficient of the $\dot{\pi}(\partial_i \pi)^2$ operator in the Lagrangian (Eq. (3.3)) does not change. Of course, this consistency is not accidental; it reflects the underlying non-linearly realized boost symmetry, which holds to all orders in the loop expansion.

Mellin transformation. In order to evaluate the time integral in Eq. (3.19), it is useful to exploit the Mellin transformations of $G_{\text{SE,SB}}(\vec{p}_E^2)$ as a function of $p_E = \sqrt{\vec{p}_E^2} > 0$, where $\vec{p}_E = (ip_0, p_i)$ is the d -dimensional Euclidean momentum. The Mellin transformation of the SE diagram is well defined and is given by

$$\tilde{G}_{\text{SE}}(z) = \int_0^\infty dp_E p_E^{z-1} G_{\text{SE}}(p_E^2) = \frac{1}{2} \frac{i\pi}{\sin(\pi z/2)} m^{z-2} \quad (0 < \operatorname{Re}(z) < 2). \quad (3.21)$$

Strictly speaking, the same transformation does not exist for $G_{\text{SB}}(p_E)$, because the integral over p_E diverges for any z . Instead, we can perform the Mellin transformation after making a suitable

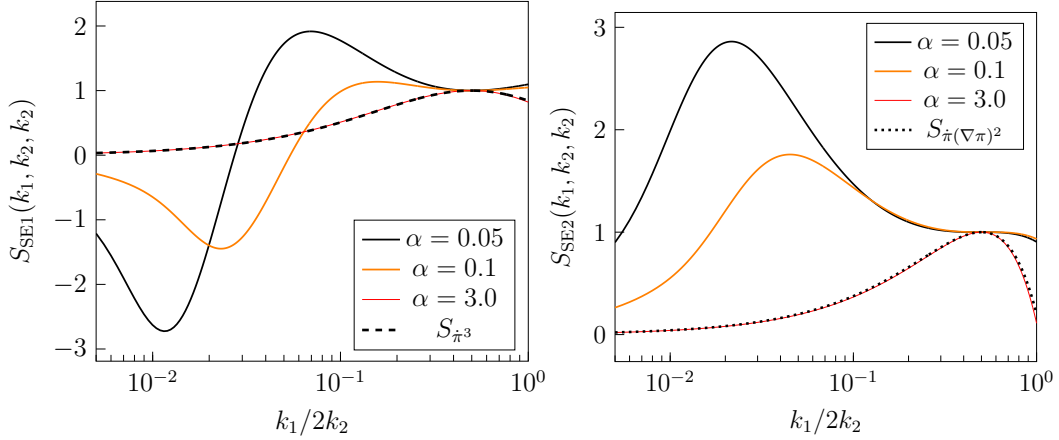


Figure 13: The shape of the bispectrum corresponding to the SE1 and SE2 diagrams, normalized to unity at the equilateral configuration ($k_1 = k_2$). For comparison, the shapes induced by the EFT operators $\dot{\pi}^3$ and $\dot{\pi}(\partial_i\pi)^2$ are also shown.

subtraction. Specifically, we define

$$\begin{aligned}\tilde{G}_{\text{SB}}(z) &= \int_0^\infty dp_E p_E^{z-1} \left[G_{\text{SB}}(p_E^2) - \frac{i}{16\pi^2} \log(m^2/\mu^2) \right] \\ &= \frac{i}{16\pi^2} \frac{\pi}{z \sin(\pi z/2)} \frac{\Gamma^2(1-z/2)}{\Gamma(2-z)} m^z \quad (-1 < \text{Re}(z) < 0).\end{aligned}\quad (3.22)$$

The inverse Mellin transformations are:

$$\begin{aligned}G_{\text{SE}}(p_E^2) &= \frac{1}{2\pi i} \int_{c-i\infty}^{c+i\infty} dz p_E^{-z} \tilde{G}_{\text{SE}}(z), \\ G_{\text{SB}}(p_E^2) &= \frac{1}{2\pi i} \int_{c-i\infty}^{c+i\infty} dz p_E^{-z} \tilde{G}_{\text{SB}}(z) + \frac{i}{16\pi^2} \log(m^2/\mu^2),\end{aligned}\quad (3.23)$$

where c is an arbitrary real number within the strip of analyticity in each case, namely $c \in (0, 2)$ for the SE graph, and $c \in (-1, 0)$ for the SB graph. Plugging the Mellin transformed graphs inside (3.19) and performing the time integral yields:

$$F_{\text{SE}}(c_s k_T, s) = \frac{H}{2m} \frac{1}{s} \text{Re} \int_{c-i\infty}^{c+i\infty} dz \frac{\Gamma(1-z)}{\sin(\pi z/2)} \left(\frac{i\alpha k_T}{s} \right)^{z-1} \quad (0 < c < 1), \quad (3.24)$$

where $\alpha = c_s m/H$. It should be noted that the integral over the conformal time is IR convergent only if $\text{Re}(z) < 1$. Therefore, the integration contour for the SE diagram had to be further restricted to $0 < c < 1$. For the one-loop diagram one finds

$$\begin{aligned}F_{\text{SB}}(c_s k_T, s) &= \frac{1}{64\pi^2} \left(\frac{m}{H} \right) \frac{1}{s} \text{Re} \int_{c-i\infty}^{c+i\infty} dz \frac{1}{\sin(\pi z/2)} \frac{z \Gamma^2(-z/2)}{1-z} \left(\frac{i\alpha k_T}{s} \right)^{z-1} \\ &\quad + \frac{1}{8\pi^2} \log(m^2/\mu^2) \frac{s}{c_s k_T} \quad (-1 < c < 0).\end{aligned}\quad (3.25)$$

Scalar-exchange seed. To derive computationally useful expressions for the seed correlators, we use the Cauchy theorem to evaluate the Mellin integrals in Eq. (3.24). We first assume $\alpha k_T/s < 1$. In this case, the original contour can be closed using an infinite arc in the right half of the complex plane. Within the resulting closed contour, the Mellin integrand of the SE diagram exhibits poles at $z = n \geq 1$. The Cauchy theorem then implies:

$$F_{\text{SE}}(c_s k_T, s) = \frac{2H}{m} \frac{1}{s} \sum_{n=1}^{\infty} \frac{1}{(2n-1)!} \left(\frac{\alpha k_T}{s} \right)^{2n-1} \left[-\log\left(\frac{\alpha k_T}{s} \right) + \psi^{(0)}(2n) \right], \quad (3.26)$$

where $\psi^{(0)}(n) (= -\gamma_E + \sum_{k=1}^{n-1} k^{-1})$ is the polygamma function of order zero. The power series representation of the SE diagram above matches the alternative formula for F_{SE} given by Eq. (2.25). Note that after taking the real part, only the poles at $z = 2n \geq 2$ have contributed to F_{SE} . Moreover, although we initially assumed $\alpha k_T/s > 1$, the series expansion actually possesses an infinite radius of convergence. This implies that Eq. (3.26) remains valid even for $\alpha k_T/s > 1$.

Scalar-bubble seed. The Mellin integrand associated with the SB diagram (Eq. (3.25)) has poles located at $z \in \{1, 2n \geq 0\}$. Summing over the residues of these poles we find:

$$F_{\text{SB}}(c_s k_T, s) = \frac{1}{16\pi^2} \left(\frac{m}{H} \right) \frac{1}{s} \sum_{n=0}^{\infty} \frac{1}{(n!)^2} \left(\frac{\alpha k_T}{s} \right)^{2n-1} \left[X_n + Y_n \log\left(\frac{\alpha k_T}{s} \right) + Z_n \log^2\left(\frac{\alpha k_T}{s} \right) \right] + \frac{1}{8\pi^2} \log(m^2/\mu^2) \frac{s}{c_s k_T},$$

where

$$\begin{aligned} X_n &= \frac{1}{(2n-1)^3} \left(4 + 4n(2n-1)^2 (\psi^{(0)}(n+1))^2 \right. \\ &\quad \left. - 2n(2n-1)^2 \psi^{(1)}(n+1) + 4(2n-1) \psi^{(0)}(n+1) \right), \\ Y_n &= -\frac{4}{(2n-1)^2} \left(2n(2n-1) \psi^{(0)}(n+1) + 1 \right), \\ Z_n &= \frac{4n}{(2n-1)}, \end{aligned} \quad (3.27)$$

where $\psi^{(1)}(n) (= \pi^2/6 - \sum_{k=1}^{n-1} k^{-2})$ is the polygamma function of order one. Similar to the SE diagram, although we performed the integration in the regime $\alpha k_T/s > 1$, the resulting power series extends to define an entire function of $\alpha k_T/s$.

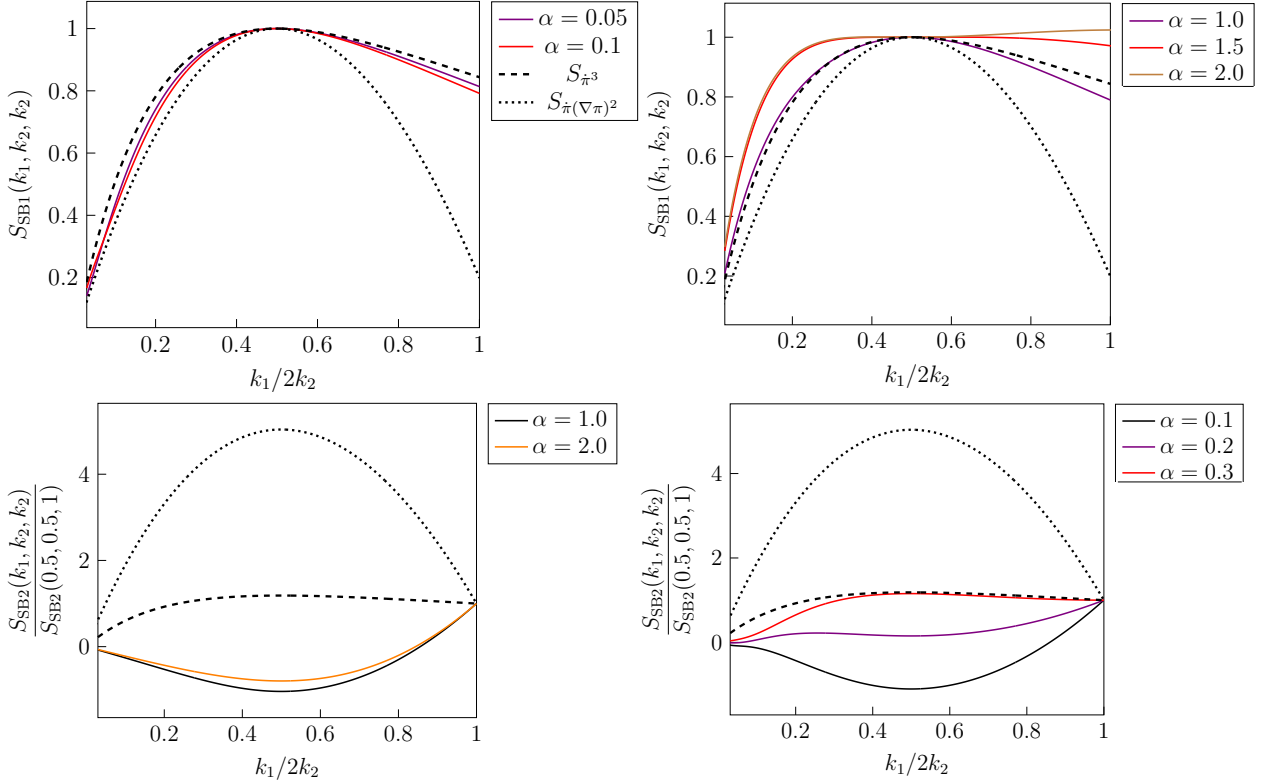


Figure 14: The shape of the bispectrum at one-loop. The plots correspond to the bispectra excluding the μ -dependent contributions highlighted in the last lines of Equations (3.37) and (3.38). For convenience, the shape is normalized to unity at $k_1 = k_2$ for Diagram SB1 and at $k_1 = 2k_2$ for Diagram SB2.

3.4 The bispectrum

We now have all the ingredients to compute the bispectrum of the curvature perturbation ζ , defined by

$$B(k_1, k_2, k_3) = \langle \zeta(\mathbf{k}_1) \zeta(\mathbf{k}_2) \zeta(\mathbf{k}_3) \rangle'. \quad (3.28)$$

At leading order in the slow-roll parameters, ζ is given by

$$\zeta \approx -H\pi = -2\pi\Delta_\zeta c_s^{3/2} \pi_c / H. \quad (3.29)$$

We find analytical expressions for all the four diagrams, by acting with the weight-shifting operators on $F_{\text{SE,SB}}$, as outlined Eq. (3.17). These results are summarised in the inserts below.

The one-loop bispectrum depends on the arbitrary renormalization scale μ . However, after renormalizing both the speed of sound c_s and the coefficient A of the cubic operator $\dot{\pi}^3$, the complete bispectrum—comprising contributions from contact cubic terms and one-loop diagrams—is guaranteed to be independent of μ . To isolate and visualize the one-loop contribution specifically, we subtract the μ -dependent parts of the bispectrum for each diagram. These subtracted components correspond to the terms highlighted in purple in the final lines of Equations (3.37) and

(3.38). Importantly, the subtracted parts are degenerate with the bispectrum contributions from the local operators $\dot{\pi}^3$ (for the SB1 diagram) and $\dot{\pi}(\partial_i\pi)^2$ (for the SB2 diagram). By subtracting these terms, we isolate the genuine one-loop contributions that are not degenerate with local EFT operators.

We first estimate the upper bounds on the size of the non-Gaussianity, which is commonly defined in terms of the bispectrum evaluated at the equilateral configuration $k_1 = k_2 = k_3$, i.e.,

$$f_{\text{NL}} = \frac{10}{9} \frac{k^6 B(k, k, k)}{(2\pi\Delta_\zeta)^4}. \quad (3.30)$$

For each diagram, perturbative unitarity bounds on the couplings, given by (3.14), (3.15) and (3.16), combined with the weak mixing assumption (3.13) (relevant for the SE1/2 graphs), impose the following upper bounds on f_{NL} :

$$\begin{aligned} f_{\text{NL}}^{\text{SE1}} &\ll \mathcal{O}(1)\sqrt{c_s}\Delta_\zeta^{-1}, & f_{\text{NL}}^{\text{SE2}} &\ll \mathcal{O}(1)/c_s^2, \\ f_{\text{NL}}^{\text{SB1}} &\ll \mathcal{O}(0.01)\Delta_\zeta^{-1}/\sqrt{c_s}, & f_{\text{NL}}^{\text{SB2}} &\ll \mathcal{O}(0.01)/c_s^2. \end{aligned} \quad (3.31)$$

Notably, the bounds on the SE1 and SB1 diagrams, both of which involve vertices containing the $\dot{\pi}^2$ operator, are relaxed by a factor of Δ_ζ^{-1} . As a result, the bispectrum generated by the SE1/2 and SB1 diagrams can reach values on the order of 10 within the perturbative framework. However, the observational constraints on the speed of sound c_s implies $f_{\text{NL}}^{\text{SB2}} \ll \mathcal{O}(10)$.

In Figures 13 and 14, we have plotted the shape of the bispectrum, defined as

$$S(k_1, k_2, k_3) \propto (k_1 k_2 k_3)^2 B(k_1, k_2, k_3), \quad (3.32)$$

as a function of $k_1/2k_2$, and for isosceles triangles (i.e., $k_3 = k_2$). The shape depends only on the parameter α , apart from an overall amplitude, which has been normalized to unity at the equilateral configuration ($k_1 = k_2 = k_3$) for the SE1, SE2, and SB1 diagrams, and at the folded configuration ($k_1 = 2k_2$) for the SB2 diagram.

The most notable feature in the tree-level shapes is the distinct resonant behavior that emerges in the squeezed limit, near $\frac{k_1}{2k_2} \sim \mathcal{O}(1)\alpha$, when α is small. As α increases and approaches $\alpha \gtrsim 1$, the resonance fades away, and the shapes of the SE1 and SE2 diagrams reduce to those generated by the local EFT operator $\dot{\pi}^3$ and $\dot{\pi}(\partial_i\pi)^2$, respectively. These resonances, referred to as the low-speed collider signal, were first introduced in [62] and fully characterized in [69]. This signal has recently been employed as an observational template for identifying signatures of heavy fields in CMB and galaxy data [146, 147].

At the one-loop level, the bispectrum shapes do not exhibit similar resonances in the squeezed limit. For $\alpha \lesssim 1$, the bispectrum corresponding to the SB1 diagram closely resembles the shape generated by the cubic operator $\dot{\pi}^3$, indicating that the signal can be effectively captured by the equilateral template. As α approaches order unity, the SB1 shape develops a plateau near the equilateral configuration. In contrast, the SB2 diagram shows markedly different behavior: for $\alpha \lesssim 0.1$, the shape displays a local minimum around the equilateral configuration, which transitions into an inflection point and then a maximum as α increases to ~ 0.3 . For α of order unity, the SB2 shape once again exhibits a local minimum near $k_1 = k_2$.

A detailed analysis of the full bispectrum shape, including its overlap with the standard local, equilateral, and orthogonal templates, is deferred to future work.

Tree-level bispectrum.

$$B_{\text{SE1}} = 4\pi^3 c_s^{1/2} \Delta_\zeta^3 \left(\frac{\rho}{\Lambda_1} \right) \times \frac{1}{\alpha k_T^2 k_1 k_2 k_3^2} \sum_{n=1}^{\infty} \frac{1}{(2n-1)!} \left(\frac{\alpha k_T}{k_3} \right)^{2n-1} (a_n + b_n \log(\alpha k_T/k_3)) + 2 \text{ perms}, \quad (3.33)$$

$$B_{\text{SE2}} = 4\pi^4 \Delta_\zeta^4 \left(\frac{\rho}{H} \right)^2 \frac{(\mathbf{k}_1 \cdot \mathbf{k}_2)}{\alpha k_1^3 k_2^3 k_3^2 k_T^2} \sum_{n=1}^{\infty} \frac{1}{(2n-1)!} \left(\frac{\alpha k_T}{k_3} \right)^{2n-1} \quad (3.34)$$

$$\times \left[\psi^{(0)}(n) k_T^2 + c_n k_{12} k_T + d_n k_1 k_2 + \log(\alpha k_T/k_3) (e_n k_1 k_2 + 2n k_{12}^2 + (1+2n) k_3 k_{12} + k_3^2) \right] + 2 \text{ perms}. \quad (3.35)$$

where

$$a_n = (4n^2 - 6n + 2)\psi^{(0)}(2n) + 3 - 4n, \quad b_n = -4n^2 + 6n - 2, \\ c_n = 1 + \psi^{(0)}(2n)(1 - 2n), \quad d_n = \psi^{(0)}(2n)(4n^2 - 6n + 2) - 4n + 3, \quad e_n = -4n^2 + 6n - 2. \quad (3.36)$$

Loop-level bispectrum.

$$B_{\text{SB1}} = \frac{\pi}{8} c_s^{-3/2} \Delta_\zeta^3 \left(\frac{gH^2}{\Lambda_2^2} \right) \times \frac{\alpha}{k_T^2 (k_1 k_2 k_3^2)} \sum_{n=0}^{\infty} \frac{1}{(n!)^2} \left(\frac{\alpha k_T}{k_3} \right)^{2n-1} \left[A_n + B_n \log \left(\frac{\alpha k_T}{k_3} \right) + 8n(n-1) \log^2 \left(\frac{\alpha k_T}{k_3} \right) \right] + 2 \text{ perms} + \frac{3\pi}{2} c_s^{-3/2} \Delta_\zeta^3 \left(\frac{gH^2}{\Lambda_2^2} \right) \log(m^2/\mu^2) \frac{1}{k_1 k_2 k_3 k_T^3}, \quad (3.37)$$

$$B_{\text{SB2}} = -\frac{\pi^2}{16} c_s^{-2} \Delta_\zeta^4 g^2 \times \frac{\alpha (k_3^2 - k_1^2 - k_2^2)}{k_1^3 k_2^3 k_3^2 k_T^2} \sum_{n=0}^{\infty} \frac{-1}{(2n-1)^3 (n!)^2} \left(\frac{\alpha k_T}{k_3} \right)^{2n-1} \left[C_n k_{12} k_T + D_n k_T^2 + E_n k_1 k_2 + \log \left(\frac{\alpha k_T}{k_3} \right) (F_n k_{12} k_T + G_n k_T^2 + H_n k_1 k_2) + \log^2 \left(\frac{\alpha k_T}{k_3} \right) (I_n k_{12} k_T + J_n k_T^2 + K_n k_1 k_2) + 2 \text{ perms} \right] + \frac{\pi^2}{4} c_s^{-1} \Delta_\zeta^4 g^2 \log(m^2/\mu^2) \left[\frac{1}{2k_1^3 k_2^3 k_3 k_T^3} (k_3^2 - k_1^2 - k_2^2) (2k_1 k_2 + k_{12} k_T + k_T^2) + 2 \text{ perms} \right], \quad (3.38)$$

where

$$\begin{aligned}
A_n &= 4 + 8n(n-1)\psi^{(0)}(n+1)^2 + 4(-4n+2)\psi^{(0)}(n+1) - 4n(n-1)\psi^{(1)}(n+1), \\
B_n &= 16n - 8 - 16n(n-1)\psi^{(0)}(n+1), \\
C_n &= 2(2n-1)^3 \left(-n\psi^{(1)}(n+1) + 2\psi^{(0)}(n+1)(n\psi^{(0)}(n+1) - 1) \right), \\
D_n &= -4 + 2(2n-1) \left(-2n(2n-1)\psi^{(0)}(n+1)^2 - 2\psi^{(0)}(n+1) + n(2n-1)\psi^{(1)}(n+1) \right), \\
E_n &= -4(2n-1)^3 \\
&\quad \times \left(1 + 2n(n-1)\psi^{(0)}(n+1)^2 + (2-4n)\psi^{(0)}(n+1) - n(n-1)\psi^{(1)}(n+1) \right), \\
F_n &= 4(2n-1)^3(1 - n\psi^{(0)}(n+1)), \quad G_n = 4(2n-1)(2n(2n-1)\psi^{(0)}(n+1) + 1), \\
H_n &= 8(2n-1)^3(1 - 2n + 2n(n-1)\psi^{(0)}(n+1)), \\
I_n &= 4n(2n-1)^3, \quad J_n = -4(2n-1)^2n, \quad K_n = -8n(n-1)(2n-1)^3. \tag{3.39}
\end{aligned}$$

4 Summary and Outlook

The established relationship between de Sitter correlators and the flat-space S-matrix, emerging at the total energy singularity of perturbative de Sitter graphs, has proven to be a valuable input in the cosmological bootstrap program. In this paper, we advanced the understanding of the connection between perturbative processes in de Sitter and flat space by formulating a novel flat-space limit for a subset of dS correlators, which are characterized by a mass gap between their external and internal legs.

We demonstrated that, in a double-scaling limit—where the external energies approach zero inversely proportional to the internal masses—the correlators undergo significant simplifications. In this regime, we derived a reduction formula that expresses the original in-in diagram in terms of the corresponding amputated diagram in flat space. Importantly, the internal lines in this limit remain massive, contrasting sharply with the conventional amplitude limit, where propagators are massless. Our results illustrate the connection between the rich structure of massive Feynman integrals and the properties of massive exchange processes in de Sitter.

We applied our MFS limit to the phenomenology of inflation by calculating the massive tree-level and one-loop exchange diagrams for the three-point function of curvature perturbations, assuming a small sound speed. Our analysis shows that the exchange of heavy fields in an intermediate mass range, specified by $H \ll m \lesssim \mathcal{O}(1)H/c_s$, leads to intriguing non-Gaussian signatures. We termed this framework the "cosmological phonon collider". The non-Gaussian shapes we identified in this setup differ notably from the oscillatory patterns typical of cosmological collider signals in the literature. We observed that the bispectrum can exhibit: (i) resonances in the mildly squeezed regime, referred to as the "low-speed collider signal" [62, 69], arising at tree level and for $\alpha = c_s m/H \ll 1$, or, depending on the vertex structure and the parameter α , (ii) a plateau or a local minimum near the equilateral configuration, at one-loop level.

There are several directions that remain to be explored.

- **On-shell massive flat-space limit.** The MFS limit proposed in this work establishes a connection between off-shell correlators and off-shell flat-space Feynman diagrams. A promising direction for further exploration involves defining an on-shell massive flat-space limit applicable directly to the original in-in diagram (without resorting to the additional energy variables ω_i). A natural proposal could be a double-scaling limit where $k_T \rightarrow 0$ and $m \rightarrow \infty$, while maintaining $k_T \times m < \infty$. One concern about such a limit is that contributions from particle production—negligible in the MFS limit due to their Boltzmann-suppressed nature—may become important. This difference arises from branch cuts introduced by particle production effects in the final correlator, leading to large exponential factors, such as $(-1)^{-im/H}$, when some of the external energies k_i take negative values. This is an unavoidable situation when $k_T \rightarrow 0$; however, it was circumvented in the MFS limit by assuming that all ω_i 's are positive real numbers. As a result of this technical difference, the structure of the MFS reduction formula might qualitatively change in an on-shell flat-space limit. We leave this direction to future work.
- **Connections with the flat-space limit of AdS/CFT.** Several frameworks have been constructed in recent years to study the flat-space limit of AdS/CFT, employing different representations of the boundary CFT, e.g., position space, Mellin space, or the conformal particle-wave expansion (see [148–154] for an incomplete list of references and [155] for a review). It would be interesting to establish concrete connections between our MFS limit and such constructions in AdS and explore other similar flat-space limits of dS.
- **Cosmological Phonon Collider.** On the phenomenological side, our results can be easily extended to include other species, such as fermions and massive vector fields. It would be interesting to explore the observational signatures of such particles especially in situations where their contributions can be enhanced, e.g. by color factors, when multiple species circle in the loop diagrams. Additionally, it would be interesting to explore whether triangle and box diagrams exhibit low-speed collider bumps, which were absent in the bubble graphs computed in this paper.

Acknowledgements

We thank Chandramouli Chowdhury, Paolo Creminelli, Claudia de Rham, Carlos Duaso Pueyo, Viola Gattus, Shota Komatsu, Arthur Lipstein, Scott Melville, Enrico Pajer, Zhehan Qin, Luca Santoni, Kostas Skenderis, David Stefanyszyn, Massimo Taronna, Andrew Tolley, Xi Tong, Toby Wiseman and Yuhang Zhu for stimulating discussions. SJ would like to thank Sébastien Renaux-Petel and Denis Werth for earlier collaborations on related topics. SJ would also like to thank the Astroparticle and Cosmology laboratory (APC) in Paris for its hospitality when parts of this work was under progress. SC would like to thank the theory group at CERN where part of this work took place. The work of SJ is supported by a Simons Investigator award 690508. SC is supported in part by the SSTFC Consolidated Grants ST/T000791/1 and ST/X000575/1 and by a Simons Investigator award 690508.

A π Effective Action from Integrating Out The Heavy Field

In this appendix we integrate out the heavy field at the level of the action and obtain a spatially non-local EFT for π (see also [62, 69, 156, 157]). We consider the simplest example in which the interactions are linear in the heavy field, namely we take

$$S_\sigma = \int d^4x \sqrt{-g} \left(-\frac{1}{2}(\partial\sigma)^2 - \frac{1}{2}m^2\sigma^2 - g \mathcal{O}[\pi(x)]\sigma \right). \quad (\text{A.1})$$

Integrating out σ induces the following effective action:

$$S_{\text{eff}} = -\frac{g^2}{2} \int d\eta d^3\mathbf{x} \frac{1}{H^4\eta^4} \mathcal{O}[\pi(\eta, \mathbf{x})] \frac{1}{\square - m^2 - i\epsilon} \mathcal{O}[\pi(\eta, \mathbf{x})]. \quad (\text{A.2})$$

The $i\epsilon$ prescription above matches with the Feynman in-out propagator. The above action is clearly non-local in both space and time. However, in the MFS limit, time derivatives acting on \mathcal{O} are suppressed compared to spatial derivatives, therefore one can expand in

$$\hat{\delta} = -\square + \nabla^2/a^2 = \eta^2\partial_\eta^2 - 2\eta\partial_\eta,$$

and re-write S_{eff} as [62]:

$$S_{\text{eff}} = -\frac{1}{2} \int d\eta d^3\mathbf{x} \frac{1}{H^4\eta^4} \mathcal{O}[\pi(\eta, \mathbf{x})] \sum_{n=0}^{\infty} (-1)^n [G(\nabla^2/a^2(\eta))\hat{\delta}]^n G(\nabla^2/a^2(\eta)) \mathcal{O}[\pi(\eta, \mathbf{x})], \quad (\text{A.3})$$

where $G(\nabla^2/a^2) = 1/(-\nabla^2/a^2 + m^2)$. The effective action above is local in time and it systematically corrects the leading order MFS effective action in Eq. (2.77).

In more detail, the typical size of $\hat{\delta}$ at the sound horizon crossing of the phonon modes, namely when $c_s|\mathbf{k}|\eta \sim H$, is of order H^2 , whereas G at the same time is of order $1/m^2$ (notice that in the MFS limit, $c_s \sim \mathcal{O}(1)H/m$). This scaling implies that the above action is organized in increasing powers of H/m .

B Spectral Decomposition

To examine the MFS limit of the bubble graph, we can resort to the spectral decomposition of the composite operator σ^2 . This decomposition allows one to write the one-loop graph given by Eq. (2.46) as a spectral integral over tree-level exchange diagrams with varied intermediate masses [58, 158]¹³.

¹³The Källén–Lehmann decomposition assumes de Sitter isometries. For the example we are considering the only relevant sector to the one-loop, spectral decomposition is the free-field Lagrangian for the massive field σ which is indeed de Sitter invariant. Consequently, the spectral decomposition of the one-loop graph is applicable even if the external legs break dS isometries, as for example in the EFT of inflation. For more generic cases, such as when the σ propagator itself break dS symmetries, the spectral representation of the one-loop diagrams is not applicable. Nevertheless, our effective action reasoning in Section 2.4 ensures that the MFS reduction formulae remains valid in all those cases.

Once translated to momentum space, the Källén–Lehmann decomposition of the scalar operator $\sigma^2(\eta, \mathbf{x})$ implies the following identity [58]:

$$\int \frac{d^d q}{(2\pi)^d} G_{\pm\pm}(|\mathbf{q}|, \eta_1, \eta_2; \mu_\sigma) G_{\pm\pm}(|\mathbf{q} - \mathbf{k}|, \eta_1, \eta_2; \mu_\sigma) = \int_0^\infty d\mu \rho_\sigma(\mu) G_{\pm\pm}(|\mathbf{k}|, \eta_1, \eta_2; \mu), \quad (\text{B.1})$$

where we have included $\mu_\sigma = \sqrt{\frac{m^2}{H^2} - \frac{d^2}{4}}$ in the propagator's arguments. μ is a similar parameter characterizing the mass spectrum appearing on the RHS above. Notice that for heavy fields the spectral integral goes over the principle series only, for which $\mu > 0$ [56]. The spectral density $\rho_\sigma(\mu)$ is given by the following formula:

$$\rho_\sigma(\mu) = \frac{\mu \sinh(\pi\mu)}{2^3 \pi^{d/2+2} \Gamma(d/2)} \frac{\Gamma^2(\frac{\Delta}{2}) \Gamma^2(\frac{d-\Delta}{2})}{\Gamma(\Delta) \Gamma(d-\Delta)} \Gamma\left(\frac{2\Delta_\sigma + \Delta - 2d}{2}\right) \Gamma\left(\frac{2\Delta_\sigma - \Delta}{2}\right) \Gamma\left(\frac{d - 2\Delta_\sigma + \Delta}{2}\right) \Gamma\left(\frac{2d - 2\Delta_\sigma + \Delta}{2}\right), \quad (\text{B.2})$$

where $\Delta = \frac{3}{2} + i\mu$ and $\Delta_\sigma = \frac{3}{2} + i\mu_\sigma$. The spectral density, written in this form, is manifestly positive and explicitly invariant under the shadow transformation $\Delta \rightarrow d - \Delta$.

We will now show that, in the flat-space limit, the combination ρ_σ/μ asymptotically approaches the spectral density appearing in the Källén–Lehmann decomposition of the σ^2 operator in Minkowski, namely

$$\rho_\sigma^{\text{mink}}(m'^2) = \frac{1}{32\pi^2} \left(1 - \frac{4m^2}{m'^2}\right)^{1/2} \theta(m'^2 - 4m^2), \quad (\text{B.3})$$

where m' is the mass parameter appearing in μ . To see this, we first note that there are three asymptotic cases in (B.2) depending on the relative size of $2\Delta_\sigma - \Delta$. For each case, we will expand the Γ functions for large or small parameters. It will come in handy to use the following approximation

$$\Gamma(A + i\mu/2) \approx \sqrt{2\pi} (|\mu|/2)^{A-1/2} e^{-\pi|\mu|/4 + \frac{i}{4}(\text{sign}(\mu)(1-2A)\pi + 2\mu(1-\log(\mu/2)))} + \mathcal{O}(1/\mu), \quad (\text{B.4})$$

which is valid for $\mu \gg 1$ and $A > 0$. Notice that the real part in the exponential depends only on the absolute value of the imaginary part of the argument of the Γ function.

The first case is when $\mu \ll \mu_\sigma$. Given that $\mu_\sigma \gg 1$, we can use the formula in Eq. (B.4) for all the Gamma functions and obtain:

$$\frac{\rho_\sigma}{\mu} \sim e^{-\frac{2\mu_\sigma}{\pi} + \mathcal{O}(1/\mu_\sigma)}, \quad |\mu| \ll 1. \quad (\text{B.5})$$

This effect is exponentially suppressed but remains nonzero. This is not surprising, as particle creation can occur in de Sitter space even below the naive particle production threshold of flat space (i.e., $m' < 2m$). The expression above, however, ceases to be valid when $|\mu - \mu_\sigma| \leq 1$. In this regime, we can approximate the Gamma function for small real δ ,

$$\Gamma(3/4 + i\delta/2) \approx \Gamma(3/4) \left(1 - \frac{\delta}{4}(2\gamma_E - \pi - \log(64)) + \mathcal{O}(\delta^2)\right) \quad (\text{B.6})$$

where this form is applied to the Gamma functions with argument $|\Delta - \Delta_\sigma|$. For the remaining terms, we use the asymptotic expression for the Gamma function from (B.4), which yields the following result,

$$\begin{aligned} \frac{\rho_\sigma(\mu)}{\mu} &= \frac{\mu \Gamma\left(\frac{3}{4}\right)^2 e^{-\frac{3\pi\mu}{2} - \pi\mu_\sigma + \mathcal{O}(\mu - \mu_\sigma)^{-2}} \sqrt{\frac{\mu}{2} + \mu_\sigma}}{8\pi^2 (4\mu^2 + 1)} \\ &\times \sinh(2\pi\mu) \left((2\gamma_E - \pi + \log(64))^2 (\mu - 2\mu_\sigma)^2 + 16 + \mathcal{O}((\mu - 2\mu_\sigma)^3) \right), \quad \text{for } |\mu - 2\mu_\sigma| \leq 1. \end{aligned} \quad (\text{B.7})$$

We observe that as μ increases, the exponential suppression, coming from the factors of μ_σ from the first limit, diminishes until it is eventually overcome. Additionally, notice that when $\mu = 2\mu_\sigma$ the spectral density is non-zero, again because the spectral density has support for particle creation below the threshold. Finally, when $|\mu - 2\mu_\sigma| \geq 1$, we have

$$\frac{\rho_\sigma(\mu)}{\mu} = \frac{2\mu^2}{\pi(1 + 4\mu^2)} \left| 1 - \frac{4\mu_\sigma^2}{4\mu^2} \right|^{1/2} \sinh(\pi\mu) e^{-\frac{\pi}{2}(3\mu + 2\mu_\sigma + |\mu - 2\mu_\sigma|) + \mathcal{O}(\mu^{-2})} \quad (|\mu - 2\mu_\sigma| \geq 1). \quad (\text{B.8})$$

In this case, we observe that the spectral density increases monotonically until μ becomes significantly larger than μ_σ , at which point it asymptotes to a constant value, resembling the behavior in Minkowski space.

The spectral density in de Sitter space differs from its Minkowski counterpart in several key aspects. First, spontaneous particle creation in de Sitter leads to a nonzero spectral density even for particles below the energy threshold, albeit with an exponentially small contribution. This contrasts with Minkowski space, where the spectral density is strictly zero below threshold, reflecting the absence of spontaneous particle creation in flat spacetime. Around the point $\mu = 2\mu_\sigma$, there is a subtle difference in de Sitter, attributed to particle creation, though this effect is minor. For $\mu \geq 2\mu_\sigma$, however, the spectral density behaves as

$$\frac{\rho_\sigma(\mu)}{\mu} \sim \frac{1}{4\pi} \left(1 - \frac{4\mu_\sigma^2}{\mu^2} \right)^{1/2} \left((1 + \mathcal{O}(e^{-2\pi\mu})) \right), \quad (\text{B.9})$$

very similarly as the Minkowski spectral density. Finally we show that in the MFS limit $\rho_\sigma(\mu)/\mu \rightarrow 8\pi\rho_\sigma^{\text{mink}}$. To see this, we reintroduce H on the expressions above, and we consider three cases previously discussed. First, in the regime where $2\mu_\sigma \ll \mu$ the spectral density scales as

$$\rho_\sigma(\mu)/\mu \sim \frac{1}{4\pi} \left(\frac{4m^2}{m'} - 1 \right)^{1/2} e^{-\frac{\pi}{H}(2m' - m)} \rightarrow 0 \quad (\text{B.10})$$

In the intermediate regime, where $|2\mu_\sigma - \mu| \leq 1$ we get that

$$\rho_\sigma(\mu)/\mu \sim e^{-\frac{\pi}{2H}(3m + m')} \sqrt{\frac{m}{H}} \rightarrow 0 \quad (\text{B.11})$$

which is also exponentially suppressed when taking the flat-space limit. Finally when $|\mu - 2\mu_\sigma| \geq 1$ we have that

$$\rho_\sigma(\mu)/\mu \sim \frac{1}{4\pi} \left(1 - \frac{4m^2}{m'} \right)^{1/2} \left(1 - \mathcal{O}(H^2/m^2) \right), \quad (\text{B.12})$$

in agreement with [29]. We can now discuss the relation between the flat space limit of the spectral density and the MFS reduction formula. Starting from the heavy graph described in (2.13), the spectral decomposition replaces the bubble diagram with the simplified expression in (B.1). In the massive field suppression (MFS) limit, where $m/H \rightarrow \infty$, the heavy graph simplifies to the standard MFS reduction formula, as shown in (2.20). In this formulation, the amputated propagator becomes:

$$G_n(p_1(\eta), \dots, p_n(\eta)) = (ig_L)(ig_R) \int \frac{d^4 \bar{q}}{(2\pi)^4} \frac{-i}{\bar{q}^2 + m^2 + i\epsilon} \frac{-i}{(\bar{q} - \sum_{i=1}^{n_L} p_i(\eta))^2 + m^2 + i\epsilon}. \quad (\text{B.13})$$

Using the spectral decomposition, this can be equivalently expressed as:

$$G_n(p_1(\eta), \dots, p_n(\eta)) = (ig_L)(ig_R) \int dm' m' \rho_\sigma^{\text{mink}}(m'^2) \frac{i}{(p_1(\eta) + \dots + p_{n_L}(\eta))^2 + m'^2}. \quad (\text{B.14})$$

Here, the spectral density $\rho_\sigma^{\text{mink}}(m'^2)$ approximates the spectral density of the one-loop graph in de Sitter, in the limit $m/H \rightarrow \infty$.

Finally, we note that the UV divergence of the spectral integral can be regularized by introducing either a hard cutoff or using dim-reg, although the specifics of this regularization procedure are not central to the analysis presented above.

References

- [1] J.M. Maldacena, *Non-Gaussian features of primordial fluctuations in single field inflationary models*, *JHEP* **05** (2003) 013 [[astro-ph/0210603](#)].
- [2] A. Achúcarro et al., *Inflation: Theory and Observations*, [2203.08128](#).
- [3] J.M. Maldacena and G.L. Pimentel, *On graviton non-Gaussianities during inflation*, *JHEP* **09** (2011) 045 [[1104.2846](#)].
- [4] A. Bzowski, P. McFadden and K. Skenderis, *Holographic predictions for cosmological 3-point functions*, *JHEP* **03** (2012) 091 [[1112.1967](#)].
- [5] P. Creminelli, *Conformal invariance of scalar perturbations in inflation*, *Phys. Rev. D* **85** (2012) 041302 [[1108.0874](#)].
- [6] I. Mata, S. Raju and S. Trivedi, *CMB from CFT*, *JHEP* **07** (2013) 015 [[1211.5482](#)].
- [7] A. Bzowski, P. McFadden and K. Skenderis, *Holography for inflation using conformal perturbation theory*, *JHEP* **04** (2013) 047 [[1211.4550](#)].
- [8] A. Bzowski, P. McFadden and K. Skenderis, *Implications of conformal invariance in momentum space*, *JHEP* **03** (2014) 111 [[1304.7760](#)].
- [9] N. Arkani-Hamed and J. Maldacena, *Cosmological Collider Physics*, [1503.08043](#).

- [10] N. Arkani-Hamed, P. Benincasa and A. Postnikov, *Cosmological Polytopes and the Wavefunction of the Universe*, [1709.02813](#).
- [11] N. Arkani-Hamed, D. Baumann, H. Lee and G.L. Pimentel, *The Cosmological Bootstrap: Inflationary Correlators from Symmetries and Singularities*, *JHEP* **04** (2020) 105 [[1811.00024](#)].
- [12] N. Arkani-Hamed and P. Benincasa, *On the Emergence of Lorentz Invariance and Unitarity from the Scattering Facet of Cosmological Polytopes*, [1811.01125](#).
- [13] D. Baumann, C. Duaso Pueyo, A. Joyce, H. Lee and G.L. Pimentel, *The cosmological bootstrap: weight-shifting operators and scalar seeds*, *JHEP* **12** (2020) 204 [[1910.14051](#)].
- [14] P. Benincasa, *Cosmological Polytopes and the Wavefunction of the Universe for Light States*, [1909.02517](#).
- [15] H. Goodhew, S. Jazayeri and E. Pajer, *The Cosmological Optical Theorem*, *JCAP* **04** (2021) 021 [[2009.02898](#)].
- [16] S. Céspedes, A.-C. Davis and S. Melville, *On the time evolution of cosmological correlators*, *JHEP* **02** (2021) 012 [[2009.07874](#)].
- [17] D. Baumann, C. Duaso Pueyo, A. Joyce, H. Lee and G.L. Pimentel, *The Cosmological Bootstrap: Spinning Correlators from Symmetries and Factorization*, *SciPost Phys.* **11** (2021) 071 [[2005.04234](#)].
- [18] P. Benincasa, A.J. McLeod and C. Vergu, *Steinmann Relations and the Wavefunction of the Universe*, *Phys. Rev. D* **102** (2020) 125004 [[2009.03047](#)].
- [19] E. Pajer, *Building a Boostless Bootstrap for the Bispectrum*, *JCAP* **01** (2021) 023 [[2010.12818](#)].
- [20] S. Jazayeri, E. Pajer and D. Stefanyszyn, *From locality and unitarity to cosmological correlators*, *JHEP* **10** (2021) 065 [[2103.08649](#)].
- [21] D. Baumann, W.-M. Chen, C. Duaso Pueyo, A. Joyce, H. Lee and G.L. Pimentel, *Linking the Singularities of Cosmological Correlators*, [2106.05294](#).
- [22] H. Goodhew, S. Jazayeri, M.H. Gordon Lee and E. Pajer, *Cutting cosmological correlators*, *JCAP* **08** (2021) 003 [[2104.06587](#)].
- [23] C. Sleight and M. Taronna, *From dS to AdS and back*, *JHEP* **12** (2021) 074 [[2109.02725](#)].
- [24] J. Bonifacio, E. Pajer and D.-G. Wang, *From amplitudes to contact cosmological correlators*, *JHEP* **10** (2021) 001 [[2106.15468](#)].
- [25] P. Benincasa, *Amplitudes meet Cosmology: A (Scalar) Primer*, [2203.15330](#).
- [26] J. Penedones, K. Salehi Vaziri and Z. Sun, *Hilbert space of Quantum Field Theory in de Sitter spacetime*, [2301.04146](#).

- [27] S. Agui Salcedo and S. Melville, *The cosmological tree theorem*, *JHEP* **12** (2023) 076 [2308.00680].
- [28] S. Albayrak, P. Benincasa and C. Duaso Pueyo, *Perturbative unitarity and the wavefunction of the Universe*, *SciPost Phys.* **16** (2024) 157 [2305.19686].
- [29] M. Loparco, J. Penedones, K. Salehi Vaziri and Z. Sun, *The Källén-Lehmann representation in de Sitter spacetime*, *JHEP* **12** (2023) 159 [2306.00090].
- [30] M.H.G. Lee, E. Pajer, M. Giroux, H.S. Hannesdottir, S. Mizera and C. Pasiecznik, *Records from the S-Matrix Marathon: A Timeless History of Time*, 9, 2024 [2410.00227].
- [31] K. Salehi Vaziri, *A non-perturbative construction of the de Sitter late-time boundary*, 2412.00183.
- [32] H. Goodhew, A. Thavanesan and A.C. Wall, *The Cosmological CPT Theorem*, 2408.17406.
- [33] D. Stefanyszyn, X. Tong and Y. Zhu, *There and Back Again: Mapping and Factorizing Cosmological Observables*, *Phys. Rev. Lett.* **133** (2024) 221501 [2406.00099].
- [34] D. Stefanyszyn, X. Tong and Y. Zhu, *Cosmological correlators through the looking glass: reality, parity, and factorisation*, *JHEP* **05** (2024) 196 [2309.07769].
- [35] S. Melville and G.L. Pimentel, *A de Sitter S-matrix from amputated cosmological correlators*, *JHEP* **08** (2024) 211 [2404.05712].
- [36] S. Melville and G.L. Pimentel, *de Sitter S matrix for the masses*, *Phys. Rev. D* **110** (2024) 103530 [2309.07092].
- [37] D. Baumann, D. Green, A. Joyce, E. Pajer, G.L. Pimentel, C. Sleight et al., *Snowmass White Paper: The Cosmological Bootstrap*, in *2022 Snowmass Summer Study*, 3, 2022 [2203.08121].
- [38] H. Gomez, R.L. Jusinkas and A. Lipstein, *Cosmological Scattering Equations*, *Phys. Rev. Lett.* **127** (2021) 251604 [2106.11903].
- [39] N. Arkani-Hamed, D. Baumann, A. Hillman, A. Joyce, H. Lee and G.L. Pimentel, *Kinematic Flow and the Emergence of Time*, 2312.05300.
- [40] N. Arkani-Hamed, D. Baumann, A. Hillman, A. Joyce, H. Lee and G.L. Pimentel, *Differential Equations for Cosmological Correlators*, 2312.05303.
- [41] D. Baumann, H. Goodhew and H. Lee, *Kinematic Flow for Cosmological Loop Integrands*, 2410.17994.
- [42] P. Benincasa, G. Brunello, M.K. Mandal, P. Mastrolia and F. Vazão, *On one-loop corrections to the Bunch-Davies wavefunction of the universe*, 2408.16386.

- [43] T.W. Grimm, A. Hoefnagels and M. van Vliet, *Structure and complexity of cosmological correlators*, *Phys. Rev. D* **110** (2024) 123531 [[2404.03716](#)].
- [44] S. Melville and E. Pajer, *Cosmological Cutting Rules*, *JHEP* **05** (2021) 249 [[2103.09832](#)].
- [45] X. Tong, Y. Wang and Y. Zhu, *Cutting Rule for Cosmological Collider Signals: A Bulk Evolution Perspective*, [2112.03448](#).
- [46] Z. Qin and Z.-Z. Xianyu, *Inflation correlators at the one-loop order: nonanalyticity, factorization, cutting rule, and OPE*, *JHEP* **09** (2023) 116 [[2304.13295](#)].
- [47] D. Ghosh, E. Pajer and F. Ullah, *Cosmological cutting rules for Bogoliubov initial states*, [2407.06258](#).
- [48] C. Sleight and M. Taronna, *Bootstrapping Inflationary Correlators in Mellin Space*, *JHEP* **02** (2020) 098 [[1907.01143](#)].
- [49] C. Sleight, *A Mellin Space Approach to Cosmological Correlators*, *JHEP* **01** (2020) 090 [[1906.12302](#)].
- [50] C. Sleight and M. Taronna, *From AdS to dS Exchanges: Spectral Representation, Mellin Amplitudes and Crossing*, [2007.09993](#).
- [51] A.J. Chopping, C. Sleight and M. Taronna, *Cosmological correlators for Bogoliubov initial states*, *JHEP* **09** (2024) 152 [[2407.16652](#)].
- [52] D. Meltzer, *Dispersion Formulas in QFTs, CFTs, and Holography*, *JHEP* **05** (2021) 098 [[2103.15839](#)].
- [53] D. Meltzer, *The inflationary wavefunction from analyticity and factorization*, *JCAP* **12** (2021) 018 [[2107.10266](#)].
- [54] S.A. Salcedo, M.H.G. Lee, S. Melville and E. Pajer, *The Analytic Wavefunction*, *JHEP* **06** (2023) 020 [[2212.08009](#)].
- [55] H. Liu, Z. Qin and Z.-Z. Xianyu, *Dispersive Bootstrap of Massive Inflation Correlators*, [2407.12299](#).
- [56] M. Hogervorst, J.a. Penedones and K.S. Vaziri, *Towards the non-perturbative cosmological bootstrap*, *JHEP* **02** (2023) 162 [[2107.13871](#)].
- [57] L. Di Pietro, V. Gorbenko and S. Komatsu, *Analyticity and Unitarity for Cosmological Correlators*, [2108.01695](#).
- [58] Z.-Z. Xianyu and H. Zhang, *Bootstrapping one-loop inflation correlators with the spectral decomposition*, *JHEP* **04** (2023) 103 [[2211.03810](#)].
- [59] L. Di Pietro, V. Gorbenko and S. Komatsu, *Cosmological Correlators at Finite Coupling*, [2312.17195](#).

- [60] D. Werth, *Spectral representation of cosmological correlators*, *JHEP* **12** (2024) 017 [2409.02072].
- [61] G. Cabass, E. Pajer, D. Stefanyszyn and J. Supel, *Bootstrapping large graviton non-Gaussianities*, *JHEP* **05** (2022) 077 [2109.10189].
- [62] S. Jazayeri and S. Renaux-Petel, *Cosmological bootstrap in slow motion*, *JHEP* **12** (2022) 137 [2205.10340].
- [63] G.L. Pimentel and D.-G. Wang, *Boostless Cosmological Collider Bootstrap*, 2205.00013.
- [64] Z. Qin and Z.-Z. Xianyu, *Helical inflation correlators: partial Mellin-Barnes and bootstrap equations*, *JHEP* **04** (2023) 059 [2208.13790].
- [65] G. Cabass, D. Stefanyszyn, J. Supel and A. Thavanesan, *On graviton non-Gaussianities in the Effective Field Theory of Inflation*, *JHEP* **10** (2022) 154 [2209.00677].
- [66] J. Bonifacio, H. Goodhew, A. Joyce, E. Pajer and D. Stefanyszyn, *The graviton four-point function in de Sitter space*, *JHEP* **06** (2023) 212 [2212.07370].
- [67] D.-G. Wang, G.L. Pimentel and A. Achúcarro, *Bootstrapping multi-field inflation: non-Gaussianities from light scalars revisited*, *JCAP* **05** (2023) 043 [2212.14035].
- [68] Z. Qin and Z.-Z. Xianyu, *Closed-form formulae for inflation correlators*, *JHEP* **07** (2023) 001 [2301.07047].
- [69] S. Jazayeri, S. Renaux-Petel and D. Werth, *Shapes of the cosmological low-speed collider*, *JCAP* **12** (2023) 035 [2307.01751].
- [70] Z.-Z. Xianyu and J. Zang, *Inflation correlators with multiple massive exchanges*, *JHEP* **03** (2024) 070 [2309.10849].
- [71] C. Duaso Pueyo and E. Pajer, *A cosmological bootstrap for resonant non-Gaussianity*, *JHEP* **03** (2024) 098 [2311.01395].
- [72] P. Chakraborty and J. Stout, *Light scalars at the cosmological collider*, *JHEP* **02** (2024) 021 [2310.01494].
- [73] P. Chakraborty and J. Stout, *Compact scalars at the cosmological collider*, *JHEP* **03** (2024) 149 [2311.09219].
- [74] S. Aoki, L. Pinol, F. Sano, M. Yamaguchi and Y. Zhu, *Cosmological correlators with double massive exchanges: bootstrap equation and phenomenology*, *JHEP* **09** (2024) 176 [2404.09547].
- [75] Z. Qin, *Cosmological Correlators at the Loop Level*, 2411.13636.
- [76] H. Liu and Z.-Z. Xianyu, *Massive Inflationary Amplitudes: Differential Equations and Complete Solutions for General Trees*, 2412.07843.

- [77] C. Chowdhury, A. Lipstein, J. Mei, I. Sachs and P. Vanhove, *The Subtle Simplicity of Cosmological Correlators*, [2312.13803](#).
- [78] C. Chowdhury, P. Chowdhury, R.N. Moga and K. Singh, *Loops, recursions, and soft limits for fermionic correlators in (A)dS*, *JHEP* **10** (2024) 202 [[2408.00074](#)].
- [79] D. Anninos, T. Anous and A. Rios Fukelman, *De Sitter at all loops: the story of the Schwinger model*, *JHEP* **08** (2024) 155 [[2403.16166](#)].
- [80] S. Raju, *New Recursion Relations and a Flat Space Limit for AdS/CFT Correlators*, *Phys. Rev. D* **85** (2012) 126009 [[1201.6449](#)].
- [81] G.L. Pimentel, L. Senatore and M. Zaldarriaga, *On Loops in Inflation III: Time Independence of zeta in Single Clock Inflation*, *JHEP* **07** (2012) 166 [[1203.6651](#)].
- [82] R. Marotta, K. Skenderis and M. Verma, *Flat space spinning massive amplitudes from momentum space CFT*, *JHEP* **08** (2024) 226 [[2406.06447](#)].
- [83] S. Weinzierl, *Feynman Integrals. A Comprehensive Treatment for Students and Researchers*, UNITEXT for Physics, Springer (2022), [10.1007/978-3-030-99558-4](#), [[2201.03593](#)].
- [84] E.E. Boos and A.I. Davydychev, *A Method of evaluating massive Feynman integrals*, *Theor. Math. Phys.* **89** (1991) 1052.
- [85] G.J. van Oldenborgh, *FF: A Package to evaluate one loop Feynman diagrams*, *Comput. Phys. Commun.* **66** (1991) 1.
- [86] G. 't Hooft and M.J.G. Veltman, *Scalar One Loop Integrals*, *Nucl. Phys. B* **153** (1979) 365.
- [87] S. Weinberg, *Quantum contributions to cosmological correlations*, *Phys. Rev. D* **72** (2005) 043514 [[hep-th/0506236](#)].
- [88] L. Senatore and M. Zaldarriaga, *On Loops in Inflation*, *JHEP* **12** (2010) 008 [[0912.2734](#)].
- [89] M. Baumgart and R. Sundrum, *De Sitter Diagrammar and the Resummation of Time*, *JHEP* **07** (2020) 119 [[1912.09502](#)].
- [90] V. Gorbenko and L. Senatore, $\lambda\phi^4$ in dS , [1911.00022](#).
- [91] D. Green and A. Premkumar, *Dynamical RG and Critical Phenomena in de Sitter Space*, *JHEP* **04** (2020) 064 [[2001.05974](#)].
- [92] L.-T. Wang, Z.-Z. Xianyu and Y.-M. Zhong, *Precision calculation of inflation correlators at one loop*, *JHEP* **02** (2022) 085 [[2109.14635](#)].
- [93] M.H.G. Lee, C. McCulloch and E. Pajer, *Leading loops in cosmological correlators*, *JHEP* **11** (2023) 038 [[2305.11228](#)].

- [94] S. Céspedes, A.-C. Davis and D.-G. Wang, *On the IR divergences in de Sitter space: loops, resummation and the semi-classical wavefunction*, *JHEP* **04** (2024) 004 [2311.17990].
- [95] M. Beneke, P. Hager and A.F. Sanfilippo, *Cosmological correlators in massless ϕ^4 -theory and the method of regions*, *JHEP* **04** (2024) 006 [2312.06766].
- [96] G. Ballesteros, J. Gambín Egea and F. Ricciardi, *Finite parts of inflationary loops*, [2411.19674](#).
- [97] X. Chen, M.H. Namjoo and Y. Wang, *Quantum Primordial Standard Clocks*, *JCAP* **02** (2016) 013 [1509.03930].
- [98] X. Chen, M.H. Namjoo and Y. Wang, *Probing the Primordial Universe using Massive Fields*, *Int. J. Mod. Phys. D* **26** (2016) 1740004 [1601.06228].
- [99] H. Lee, D. Baumann and G.L. Pimentel, *Non-Gaussianity as a Particle Detector*, *JHEP* **12** (2016) 040 [1607.03735].
- [100] X. Chen, Y. Wang and Z.-Z. Xianyu, *Standard Model Background of the Cosmological Collider*, *Phys. Rev. Lett.* **118** (2017) 261302 [1610.06597].
- [101] X. Chen, Y. Wang and Z.-Z. Xianyu, *Standard Model Mass Spectrum in Inflationary Universe*, *JHEP* **04** (2017) 058 [1612.08122].
- [102] A. Kehagias and A. Riotto, *On the Inflationary Perturbations of Massive Higher-Spin Fields*, *JCAP* **07** (2017) 046 [1705.05834].
- [103] X. Chen, W.Z. Chua, Y. Guo, Y. Wang, Z.-Z. Xianyu and T. Xie, *Quantum Standard Clocks in the Primordial Trispectrum*, *JCAP* **05** (2018) 049 [1803.04412].
- [104] S. Kumar and R. Sundrum, *Cosmological Collider Physics and the Curvaton*, *JHEP* **04** (2020) 077 [1908.11378].
- [105] T. Liu, X. Tong, Y. Wang and Z.-Z. Xianyu, *Probing P and CP Violations on the Cosmological Collider*, *JHEP* **04** (2020) 189 [1909.01819].
- [106] L.-T. Wang and Z.-Z. Xianyu, *Gauge Boson Signals at the Cosmological Collider*, *JHEP* **11** (2020) 082 [2004.02887].
- [107] C.M. Sou, X. Tong and Y. Wang, *Chemical-potential-assisted particle production in FRW spacetimes*, *JHEP* **06** (2021) 129 [2104.08772].
- [108] L. Li, S. Lu, Y. Wang and S. Zhou, *Cosmological Signatures of Superheavy Dark Matter*, *JHEP* **07** (2020) 231 [2002.01131].
- [109] S. Lu, Y. Wang and Z.-Z. Xianyu, *A Cosmological Higgs Collider*, *JHEP* **02** (2020) 011 [1907.07390].
- [110] Q. Lu, M. Reece and Z.-Z. Xianyu, *Missing scalars at the cosmological collider*, *JHEP* **12** (2021) 098 [2108.11385].

- [111] L. Pinol, S. Aoki, S. Renaux-Petel and M. Yamaguchi, *Inflationary flavor oscillations and the cosmic spectroscopy*, *Phys. Rev. D* **107** (2023) L021301 [2112.05710].
- [112] Y. Cui and Z.-Z. Xianyu, *Probing Leptogenesis with the Cosmological Collider*, 2112.10793.
- [113] X. Tong and Z.-Z. Xianyu, *Large spin-2 signals at the cosmological collider*, *JHEP* **10** (2022) 194 [2203.06349].
- [114] M. Reece, L.-T. Wang and Z.-Z. Xianyu, *Large-Field Inflation and the Cosmological Collider*, 2204.11869.
- [115] X. Chen, R. Ebadi and S. Kumar, *Classical Cosmological Collider Physics and Primordial Features*, 2205.01107.
- [116] Z. Qin and Z.-Z. Xianyu, *Phase Information in Cosmological Collider Signals*, 2205.01692.
- [117] N. Craig, S. Kumar and A. McCune, *An effective cosmological collider*, *JHEP* **07** (2024) 108 [2401.10976].
- [118] J. Quintin, X. Chen and R. Ebadi, *Fingerprints of a non-inflationary universe from massive fields*, *JCAP* **09** (2024) 026 [2405.11016].
- [119] A. Bodas, E. Broadberry and R. Sundrum, *Grand Unification at the Cosmological Collider with Chemical Potential*, 2409.07524.
- [120] F. Gasparotto, P. Mazloumi and X. Xu, *Differential equations for tree-level cosmological correlators with massive states*, 2411.05632.
- [121] E. Pajer, D.-G. Wang and B. Zhang, *The UV Sensitivity of Axion Monodromy Inflation*, 2412.05762.
- [122] S. Jazayeri, S. Renaux-Petel, X. Tong, D. Werth and Y. Zhu, *Parity Violation from Emergent Non-Locality During Inflation*, 2308.11315.
- [123] X. Chen, Y. Wang and Z.-Z. Xianyu, *Schwinger-Keldysh Diagrammatics for Primordial Perturbations*, *JCAP* **12** (2017) 006 [1703.10166].
- [124] S.A. Salcedo, T. Colas and E. Pajer, *The open effective field theory of inflation*, *JHEP* **10** (2024) 248 [2404.15416].
- [125] C.P. Burgess, T. Colas, R. Holman, G. Kaplanek and V. Vennin, *Cosmic purity lost: perturbative and resummed late-time inflationary decoherence*, *JCAP* **08** (2024) 042 [2403.12240].
- [126] C.P. Burgess, T. Colas, R. Holman and G. Kaplanek, *Does decoherence violate decoupling?*, 2411.09000.
- [127] D. Green and G. Sun, *Effective Field Theory and In-In Correlators*, 2412.02739.

- [128] S. Renaux-Petel, X. Tong, D. Werth and Y. Zhu, *in preparation*, .
- [129] S. Bhowmick, D. Ghosh and F. Ullah, *Bispectrum at 1-loop in the Effective Field Theory of Inflation*, *JHEP* **10** (2024) 057 [[2405.10374](#)].
- [130] L.E. Parker and D. Toms, *Quantum Field Theory in Curved Spacetime: Quantized Field and Gravity*, Cambridge Monographs on Mathematical Physics, Cambridge University Press (8, 2009), [10.1017/CBO9780511813924](#).
- [131] D. Baumann and D. Green, *Signatures of Supersymmetry from the Early Universe*, *Phys. Rev. D* **85** (2012) 103520 [[1109.0292](#)].
- [132] A. Achucarro, J.-O. Gong, S. Hardeman, G.A. Palma and S.P. Patil, *Effective theories of single field inflation when heavy fields matter*, *JHEP* **05** (2012) 066 [[1201.6342](#)].
- [133] A. Achucarro, V. Atal, S. Cespedes, J.-O. Gong, G.A. Palma and S.P. Patil, *Heavy fields, reduced speeds of sound and decoupling during inflation*, *Phys. Rev. D* **86** (2012) 121301 [[1205.0710](#)].
- [134] T.S. Bunch and L. Parker, *Feynman Propagator in Curved Space-Time: A Momentum Space Representation*, *Phys. Rev. D* **20** (1979) 2499.
- [135] D.V. Vassilevich, *Heat kernel expansion: User's manual*, *Phys. Rept.* **388** (2003) 279 [[hep-th/0306138](#)].
- [136] I.G. Avramidi, *Covariant methods for the calculation of the effective action in quantum field theory and investigation of higher derivative quantum gravity*, other thesis, 1986, [[hep-th/9510140](#)].
- [137] A. Nicolis, R. Penco, F. Piazza and R.A. Rosen, *More on gapped Goldstones at finite density: More gapped Goldstones*, *JHEP* **11** (2013) 055 [[1306.1240](#)].
- [138] A. Nicolis, R. Penco and R.A. Rosen, *Relativistic Fluids, Superfluids, Solids and Supersolids from a Coset Construction*, *Phys. Rev. D* **89** (2014) 045002 [[1307.0517](#)].
- [139] A. Nicolis, R. Penco, F. Piazza and R. Rattazzi, *Zoology of condensed matter: Framids, ordinary stuff, extra-ordinary stuff*, *JHEP* **06** (2015) 155 [[1501.03845](#)].
- [140] A. Joyce, A. Nicolis, A. Podo and L. Santoni, *Integrating out beyond tree level and relativistic superfluids*, *JHEP* **09** (2022) 066 [[2204.03678](#)].
- [141] PLANCK collaboration, *Planck 2018 results. VI. Cosmological parameters*, [1807.06209](#).
- [142] PLANCK collaboration, *Planck 2018 results. IX. Constraints on primordial non-Gaussianity*, *Astron. Astrophys.* **641** (2020) A9 [[1905.05697](#)].
- [143] L. Bordin, P. Creminelli, A. Khmelnitsky and L. Senatore, *Light Particles with Spin in Inflation*, *JCAP* **10** (2018) 013 [[1806.10587](#)].

- [144] L. Pinol, S. Renaux-Petel and D. Werth, *The Cosmological Flow: A Systematic Approach to Primordial Correlators*, [2312.06559](#).
- [145] T. Grall and S. Melville, *Inflation in Motion: Unitarity Constraints in Effective Field Theories with Broken Lorentz Symmetry*, [2005.02366](#).
- [146] W. Sohn, D.-G. Wang, J.R. Fergusson and E.P.S. Shellard, *Searching for cosmological collider in the Planck CMB data*, *JCAP* **09** (2024) 016 [[2404.07203](#)].
- [147] G. Cabass, O.H.E. Philcox, M.M. Ivanov, K. Akitsu, S.-F. Chen, M. Simonović et al., *BOSS Constraints on Massive Particles during Inflation: The Cosmological Collider in Action*, [2404.01894](#).
- [148] J. Polchinski, *S matrices from AdS space-time*, [hep-th/9901076](#).
- [149] S.B. Giddings, *Flat space scattering and bulk locality in the AdS / CFT correspondence*, *Phys. Rev. D* **61** (2000) 106008 [[hep-th/9907129](#)].
- [150] M. Gary, S.B. Giddings and J. Penedones, *Local bulk S-matrix elements and CFT singularities*, *Phys. Rev. D* **80** (2009) 085005 [[0903.4437](#)].
- [151] I. Heemskerk, J. Penedones, J. Polchinski and J. Sully, *Holography from Conformal Field Theory*, *JHEP* **10** (2009) 079 [[0907.0151](#)].
- [152] A.L. Fitzpatrick, E. Katz, D. Poland and D. Simmons-Duffin, *Effective Conformal Theory and the Flat-Space Limit of AdS*, *JHEP* **07** (2011) 023 [[1007.2412](#)].
- [153] J. Maldacena, D. Simmons-Duffin and A. Zhiboedov, *Looking for a bulk point*, *JHEP* **01** (2017) 013 [[1509.03612](#)].
- [154] S. Komatsu, M.F. Paulos, B.C. Van Rees and X. Zhao, *Landau diagrams in AdS and S-matrices from conformal correlators*, *JHEP* **11** (2020) 046 [[2007.13745](#)].
- [155] Y.-Z. Li, *Notes on flat-space limit of AdS/CFT*, *JHEP* **09** (2021) 027 [[2106.04606](#)].
- [156] R. Gwyn, G.A. Palma, M. Sakellariadou and S. Sypsas, *Effective field theory of weakly coupled inflationary models*, *JCAP* **1304** (2013) 004 [[1210.3020](#)].
- [157] R. Gwyn, G.A. Palma, M. Sakellariadou and S. Sypsas, *On degenerate models of cosmic inflation*, *JCAP* **1410** (2014) 005 [[1406.1947](#)].
- [158] D. Marolf and I.A. Morrison, *The IR stability of de Sitter: Loop corrections to scalar propagators*, *Phys. Rev. D* **82** (2010) 105032 [[1006.0035](#)].